1-1-1982

Effects of neutron flux gradient and detector-vibrator geometry on the local-global responses of the UTR-10 reactor

Robert John Borland
Iowa State University

Effects of neutron flux gradient and detector-vibrator geometry on the local-global responses of the UTR-10 reactor

by

Robert John Borland

A Thesis Submitted to the
Graduate Faculty in Partial Fulfillment of the
Requirements for the Degree of
MASTER OF SCIENCE

Major: Nuclear Engineering

Iowa State University
Ames, Iowa

1982

TABLE OF CONTENTS

LIST OF TABLES

LIST OF FIGURES

I. INTRODUCTION

It has long been recognized that the noise generated by a vibrating neutron absorber, such as a fuel rod or control rod, is highly space-dependent and that the localization of such a vibrating absorber could be achieved by analyzing the neutron noise seen by in-core neutron detectors [1-9]. Although the technique of using neutron noise analysis to characterize and localize reactor core component vibrations has been explored a great deal from a theoretical standpoint, there has been little experimental work performed in this field. One of the few studies in this area was carried out by Al-Ammar [1] with the UTR-10 reactor at Iowa State University.

Al-Ammar designed an apparatus that replaced the central vertical stringer (CVS) in the reactor core. The apparatus consisted of a vibrating Plexiglas strip with a piece of cadmium attached to one end acting as an absorber. Two BF_3 neutron detectors located close to the vibrating absorber detected the fluctuations created in the neutron flux by the moving absorber. A microswitch was used to indicate the position of the vibrator. Using data obtained with this apparatus, Al-Ammar observed that the noise generated by the absorber was composed of two parts: a space-dependent or "local" component, and a reactivity or "global" component, both of which were predicted by theory [2-7].

Al-Ammar's apparatus was somewhat limited, as he could only make the vibrator move along the line between the two detectors. He had no way to examine the detector response for an absorber moving, for example, perpendicular to a line between the two detectors. Also, several design flaws hampered Al-Ammar's work. One problem was that the Plexiglas strip, being relatively flexible, had a tendency to "whip" at higher frequencies, causing one end to lag behind the other. Since the microswitch and the absorber were at opposite ends of the Plexiglas strip, the microswitch signal did not accurately reflect the position of the absorber. Also, the microswitch provided only a very discrete observation of the motion of the vibrator; the switch was on when the vibrator was in one position and off when the vibrator was anywhere else. Although analysis of the detector signals did not require a knowledge of the absorber position, the position-measuring device was still useful in testing the apparatus and in detecting apparatus malfunctions. Al-Ammar suggested that if a stiffer vibrator material and a better position-measuring device were used, better results might be obtained.

There was still a great deal of new information that could be obtained by placing an apparatus similar to Al-Ammar's in the CVS. Therefore, the objectives of this research were threefold:

1. To design, construct, and test a new apparatus similar to Al-Ammar's, but including several modifications and refinements to improve data quality and increase the versatility of the apparatus;
2. To use the apparatus to verify the local and global effects that Al-Ammar observed;
3. To investigate the reactor response to a vibrating absorber that is moving perpendicular to a line between the two detectors.

A theoretical analysis using one- and two-dimensional diffusion theory was carried out so that the effects of different thermal neutron flux gradients on the reactor response would be understood. A phenomenological analysis was also carried out based on how the detectors would respond to the noise generated by the moving absorber. The results of this last analysis were later used in analyzing the experiment data that were obtained. The apparatus was operated in four different modes in the CVS: two modes with the absorber moving along the line between the two detectors and two modes with it moving perpendicular to the line between the detectors. The data obtained were analyzed with a frequency spectrum analyzer, and a microcomputer was used to calculate auto-power spectral densities and local-to-global ratios. The results were compared to the theoretical predictions and to the results of Al-Ammar's research.

II. LITERATURE REVIEW

There has been a great deal of theoretical work [2-8] and, to a lesser extent, experimental work [1,9] performed over the past few years in analyzing reactor core component vibrations using neutron flux noise analysis.

One of the most important theoretical developments was that of the frequency-dependent detector adjoint function by Van Dam [2]. Although that specific application of the detector adjoint function was in regard to noise induced by steam voids in boiling water reactors, Van Dam was able to show that a noise source in a reactor generated two effects: a space-dependent or "local" effect created by movement of the flux depression and a space-independent reactivity or "global" effect. Similar theoretical work on BWR noise was done by Behringer, Kosaly, and Kostic [3], and this effort reinforced Van Dam's work.

A point reactor treatment of the noise induced by a vibrating absorber was conducted by Pazsit [4]. He concluded that the noise field generated by a vibrating absorber is highly space-dependent and differs greatly from the noise generated by a stationary absorber of varying strength. In a later work [5], Pazsit used a two-energy group model and Van Dam's detector adjoint function to verify the above conclusions. Pazsit's analysis was performed only in one dimension, but Pazsit and Analytis [6] developed a two-dimensional

model using the Green's function technique. They concluded that if the equilibrium position of a vibrating absorber is known, it should be possible to reconstruct the trajectory of the absorber from the signals from two neutron detectors. However, they stated that the problem of localizing a vibrating absorber whose equilibrium position is not known is much more difficult in theory and might well be impossible in practice due to the large number of noise sources present in a reactor core.

Analytis [7] also used a Green's function approach for a three-dimensional analysis which verified the earlier study performed by Analytis and Pazsit [6], but he concluded that extensive numerical investigation of his three-dimensional model was required.

Both theoretical [8] and experimental [1,9] analyses have been performed on the UTR-10 reactor at Iowa State University. Salih [8] used WHIRLAWAY to calculate neutron fluxes and detector adjoint functions for various detector locations in the UTR-10. He concluded that the central vertical stringer (CVS) and the space next to the north core tank were suitable detector locations for measurement purposes.

Al-Ammar [1] constructed an apparatus which could be inserted into the UTR-10 in place of the CVS. His apparatus consisted of a one-dimensional vibrating absorber and two neutron detectors. With this apparatus, he obtained experimental data which verified the local-global hypothesis discussed by Pazsit [5]. Al-Ammar found

that the local effect was about 3.7 times greater than the global effect for an absorber vibrating in the north-south plane at a frequency of about 1.0 Hertz. For an absorber moving in the east-west plane, the ratio was much higher due to the smaller thermal flux gradient in that direction. Along with Danofsky, Al-Ammar examined the usefulness of the normalized cross-power spectral density (NCPSD) as a tool for localizing the position of a moving absorber [9].

III. MATHEMATICAL ANALYSIS OF THE VIBRATING ABSORBER PROBLEM

In this section, a theoretical groundwork will be laid for the vibrating absorber problem. This groundwork will include not only one- and two-dimensional analytic models and their implications, but also several "phenomenological" models for examining data that could be generated by some different experimental modes examined in the UTR-10 reactor.

A. One-Dimensional Response

It is desirable to determine the response of a reactor to a vibrating absorber oscillating in one dimension, since this is one of the possible modes of experimentation. This response has been calculated using a number of different methods [2-5], but in this discussion only the highlights of the derivation will be presented. A more detailed derivation is available in Appendix A.

Written in operator notation, the two-energy group, one-dimensional diffusion equations are [1]

$$\underline{\underline{L}}(x,t)\underline{\phi}(x,t) = 0. \tag{3.1}$$

It may be assumed that only the thermal absorption cross section, which is included in $\underline{\underline{L}}$, is perturbed by the vibration. The cross section may then be stated as [5]

$$\Sigma_{a2}(t) = \Sigma_{a2o} + \delta\Sigma_{a2}(t). \tag{3.2}$$

This fluctuation will cause the fast and thermal fluxes and the delayed neutron precursor concentration to be perturbed in a similar fashion.

The perturbed variables are substituted into Equation (3.1); these equations are then linearized and converted to the frequency domain. This yields

$$\underline{\underline{L}}(x,\omega)\Delta\underline{\phi}(x,\omega) = \underline{S}(x,\omega)\,, \tag{3.3}$$

where $\Delta\underline{\phi}$ is the flux perturbation vector, and $\underline{S}$ describes the frequency dependent cross section perturbation.

The adjoint function technique [2] is used to solve Equation (3.3). This gives

$$\underline{\underline{L}}^{+}(x,\omega)\underline{\psi}^{+}(x,\omega) = \underline{\Sigma}_{d}(x,\omega)\,, \tag{3.4}$$

where $\underline{\underline{L}}^{+}$ is the 2x2 adjoint operator, $\underline{\psi}^{+}$ is the adjoint flux vector, and $\underline{\Sigma}_{d}$ is the cross section vector for a thermal detector of magnitude Q located at $x=x_o$. Thus,

$$\underline{\Sigma}_{d}(x,\omega) = \begin{bmatrix} 0 \\ Q\delta(x-x_o) \end{bmatrix}\,. \tag{3.5}$$

Next, the inner products of Equations (3.3) and (3.4) with $\underline{\psi}^{+}$ and $\Delta\underline{\phi}$, respectively, are calculated. From the definition of the adjoint [10], it can be shown the left-hand sides of the two inner product equations are equal. Thus, the right-hand sides may be

equated and, using integral representation of the inner products [11], written as

$$\int_x \Delta\underline{\phi}(x,\omega)^T \underline{\Sigma}_d(x,\omega)dx = \int_x \underline{S}(x,\omega)^T \underline{\psi}^+(x,\omega)dx. \tag{3.6}$$

Equation (3.5) is substituted into Equation (3.6), which is solved for the perturbed thermal flux, yielding

$$\Delta\phi_2(x_o,\omega) = \frac{1}{Q}\int_x \Delta\Sigma_{a2}(\omega)\phi_2(x)\psi_2^+(x,x_o,\omega)dx. \tag{3.7}$$

Equation (3.7) describes the response of a thermal detector located at $x=x_o$ to a thermal absorption perturbation somewhere in the reactor.

The vibrating absorber may be described as a thermal absorbing plate located at x_p, vibrating with an amplitude of $\pm\varepsilon$, and having an absorption strength of γ. Thus, [5]

$$\delta\Sigma_{a2}(t) = \gamma\left\{\delta[x-x_p-\varepsilon(t)] - \delta(x-x_p)\right\}. \tag{3.8}$$

Equation (3.8) is substituted into Equation (3.7) and then the space integral is carried out. Instead of using the Fourier transform to bring all terms into the frequency domain at this point, the resulting equation is expanded in a Taylor series of $\varepsilon(t)$ and all terms greater than first order in $\varepsilon(t)$ are ignored. The $\varepsilon(t)$ term then is transformed into the frequency domain, with the result being [5]

$$\Delta\phi_2(x_o,\omega) = \frac{\gamma}{Q}\left[\phi_2(x_p)\left.\frac{\partial\psi_2(x,x_o,\omega)}{\partial x}\right|_{x=x_p-0}\right.$$

$$\left. + \psi_2^+(x_p,x_o,\omega)\left.\frac{\partial\phi_2(x)}{\partial x}\right|_{x=x_p}\right]\varepsilon(\omega). \qquad (3.9)$$

Equation (3.9) describes the two basic components that comprise the detector response. The first component depends upon the static thermal flux and the thermal adjoint gradient; it describes the response due to the movement of the local flux depression around the absorber and, consequently, it is called the "local" effect. The second term is dependent upon the thermal adjoint and the thermal flux gradient; it describes the reactivity effect generated by the absorber moving through a flux gradient. Since this effect is space independent, it is called the "global" effect. These two effects can add to, or subtract from, each other, depending upon the signs of the gradient terms in Equation (3.9).

One particularly interesting case is that of detectors symmetrically placed about a vibrator, as shown in Figure 3.1. The static thermal flux gradient is such that the flux increases from right to left. As the vibrating absorber moves toward the left, the left detector not only sees the local flux depression, but it also detects a drop in the entire reactor flux due to a negative reactivity insertion created by the absorber moving up the flux gradient. The right detector also sees the global flux depression,

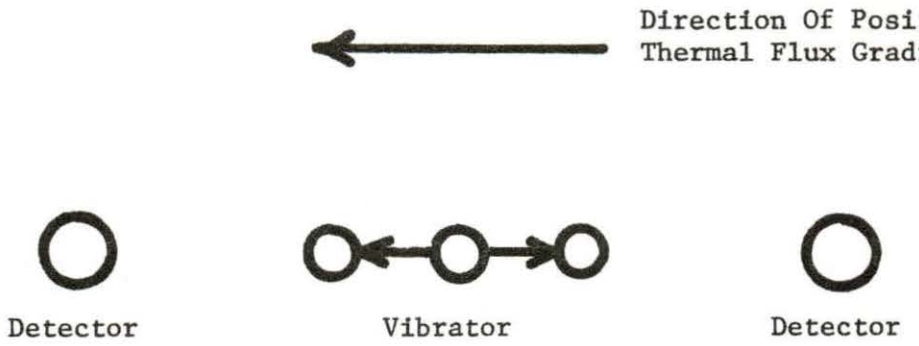

(a)

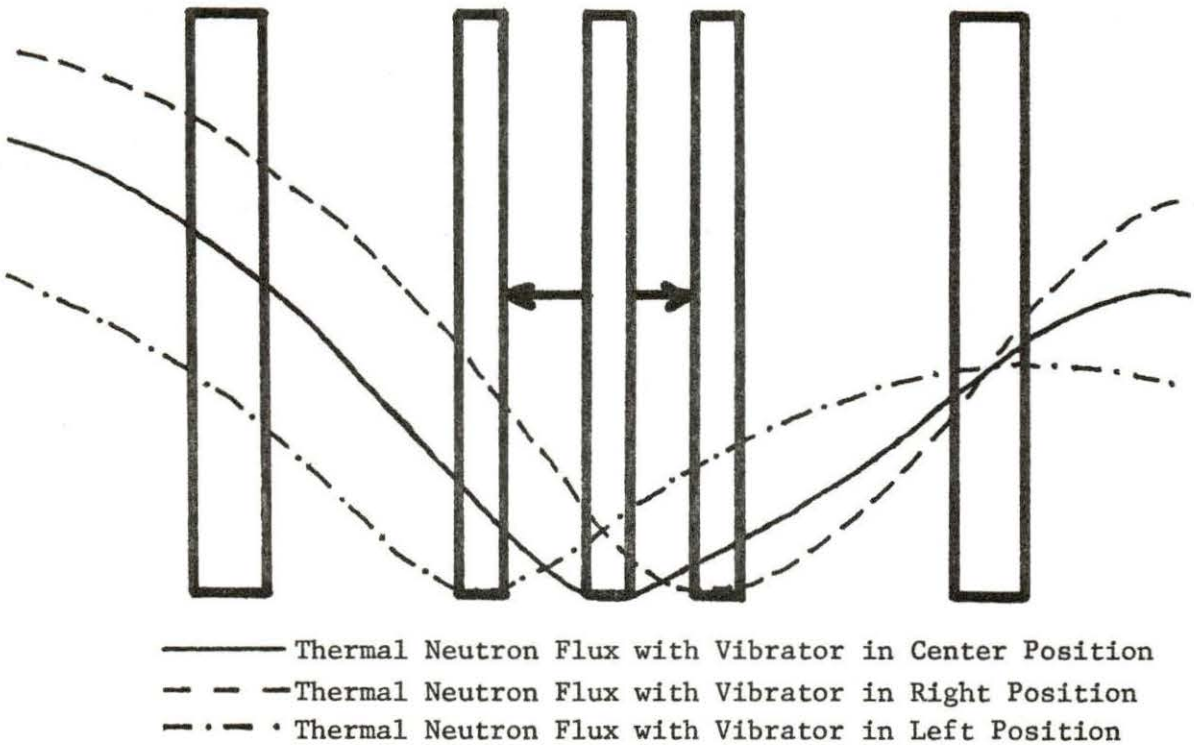

(b)

Figure 3.1. Configuration and reactor response for the special one-dimensional case

but since the absorber is moving away from the right detector, it also sees an increase in the "local" flux. If the magnitudes of both the local and global effects are about the same, the two effects would cancel each other at the right detector, and that detector would see no change in the thermal flux.

B. Two-Dimensional Response

The derivation of the response of a detector to a vibrating absorber moving in two dimensions is similar to the one-dimensional derivation [6], so the derivation will be omitted here.

For an absorber of strength γ located at $x=x_p$, $y=y_p$, and vibrating so that the vibration amplitude may be described by

$$\varepsilon(t) = \varepsilon_x(t) + \varepsilon_y(t), \tag{3.10}$$

the response of a detector located at $x=x_o$, $y=y_o$, and with magnitude Q is [6]

$$\Delta\phi_2(x_o,y_o,\omega) = \frac{\gamma}{QM^2\Sigma_{a2}} \left\{ \left[\phi_2(x_p,y_p,\omega) \frac{\partial G_2(x_p,y_p,x_o,y_o,\omega)}{\partial x_p} + G_2(x_p,y_p,x_o,y_o,\omega) \frac{\partial \phi_2(x_p,y_p,\omega)}{\partial x_p} \right] \varepsilon_x(\omega) + \left[\phi_2(x_p,y_p,\omega) \frac{\partial G_2(x_p,y_p,x_o,y_o,\omega)}{\partial y_p} \right. \right.$$

$$+ G_2(x_p,y_p,x_o,y_o,\omega) \left.\frac{\partial \phi_2(x_p,y_p,\omega)}{\partial y_p}\right] \varepsilon_y(\omega) \Bigg\}, \qquad (3.11)$$

where M^2 is the thermal migration area and G_2 refers to the two-dimensional Green's function solution to the original differential equation.

As in the one-dimensional response, there are local and global components in the two-dimensional response as well. Also, the same type of cancellation effects that can occur in the one-dimensional problem is possible here.

Another interesting special case is shown in Figure 3.2. In this reference system, the vibrator is located at the origin and is vibrating along the y-axis. The two detectors are located symmetrically about the y-axis on the x-axis. Since the vibrator moves only in the y-direction, $\varepsilon_x(\omega) = 0$, causing the first two partial derivative terms in Equation (3.11) to drop out. Since the detectors are symmetrically placed about the y-axis, and the remaining terms in Equation (3.11) are even about the y-axis, both detectors should see the same flux perturbation. The manner in which the local and global effects combine, however, is considerably different than the one-dimensional case. Figure 3.3 shows a graphical representation of the local and global effects and their summation for a vibrator moving at a constant frequency. Since the detectors

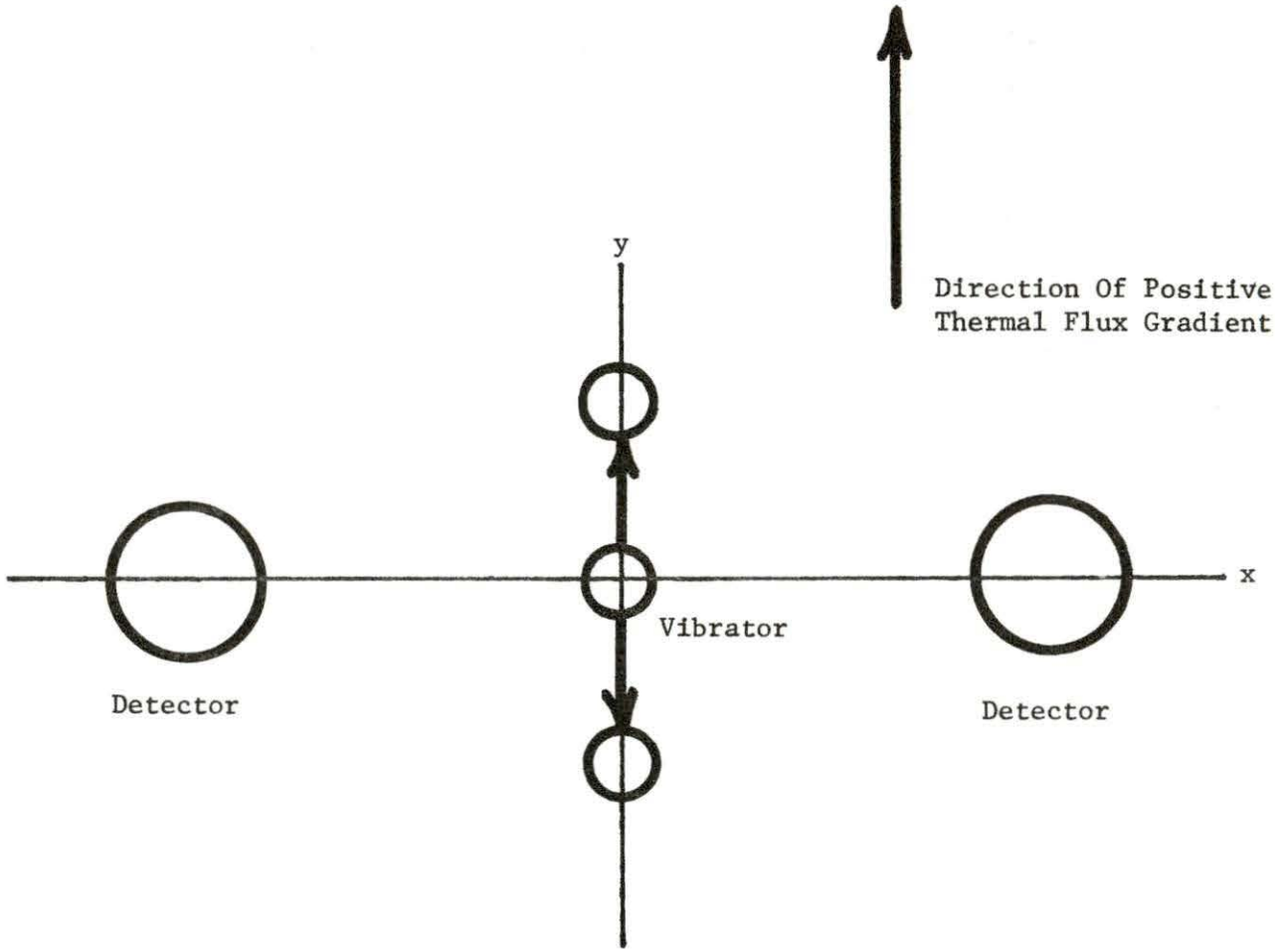

Figure 3.2. Configuration for the special two-dimensional case

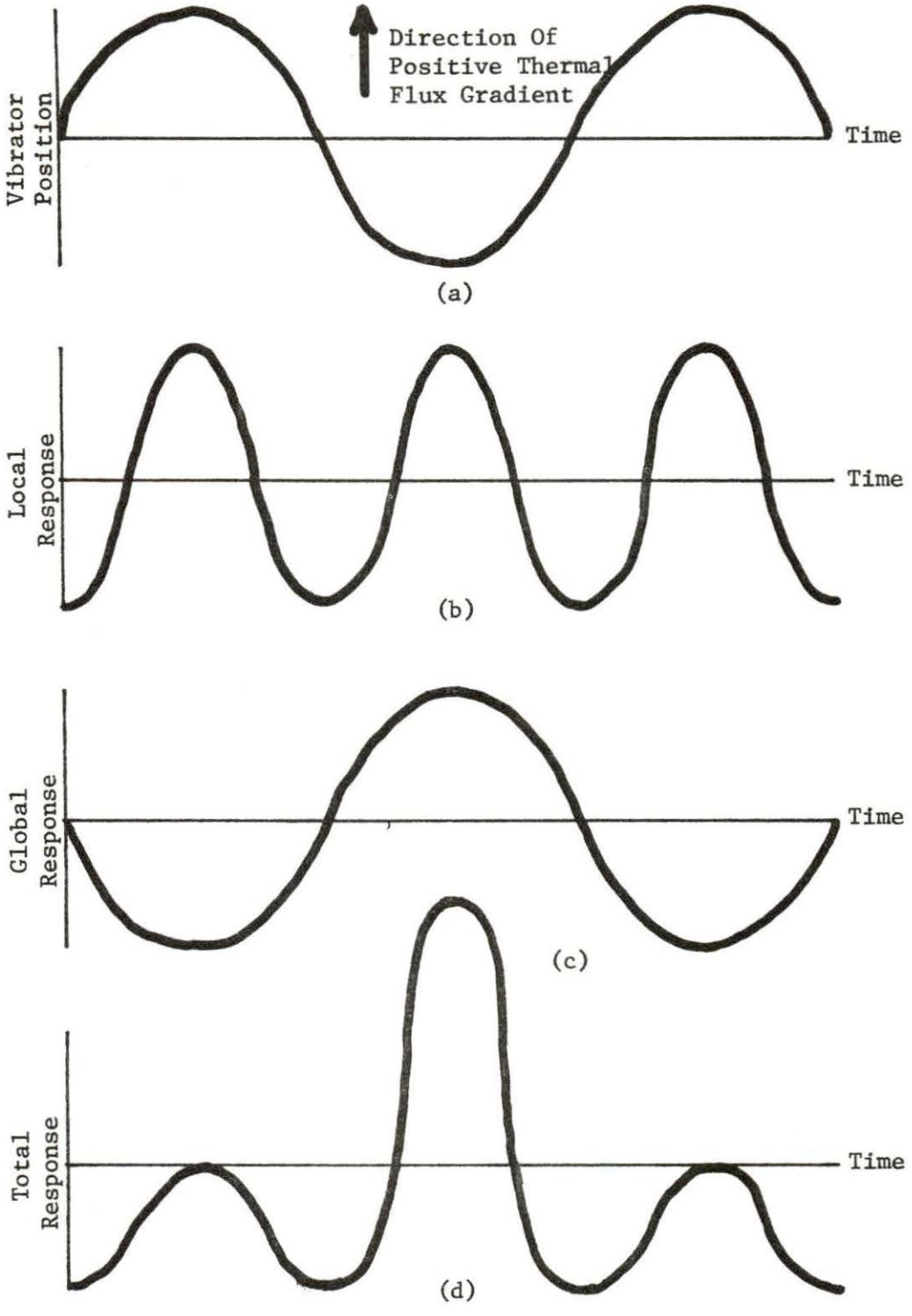

Figure 3.3. Reactor response for the special two-dimensional case for arbitrary local and global magnitudes

see a minimum in the local component whenever the vibrator is at the origin, they will detect the local component as having twice the frequency of the vibrator. However, the global component is independent of detector position and, consequently, will be at the same frequency as the vibrator. The total effect will be a summation of the two components, as shown in Figure 3.3. However, this is true only if the thermal flux gradient has a non-zero component in the y-direction. If the only non-zero gradient component is in the x-direction, the detectors would see only a local effect.

C. Phenomenological Analysis

Earlier, a one-dimensional case was discussed where two detectors could be placed symmetrically about the vibrator (see Fig. 3.1). This case turns out to be one that could easily be examined in an experimental analysis, thus making it desirable to model the detector signals from a phenomenological approach.

Since the global component is actually a reactivity effect, it may be modeled as the zero-power reactor transfer function [1], making the global effect complex and allowing it to be described by a magnitude and a phase angle. To simplify the analysis, it is assumed that the local component is real, and, therefore, has no phase, and that the global phase is measured relative to the local component. Figure 3.4 shows a graphical representation of this model.

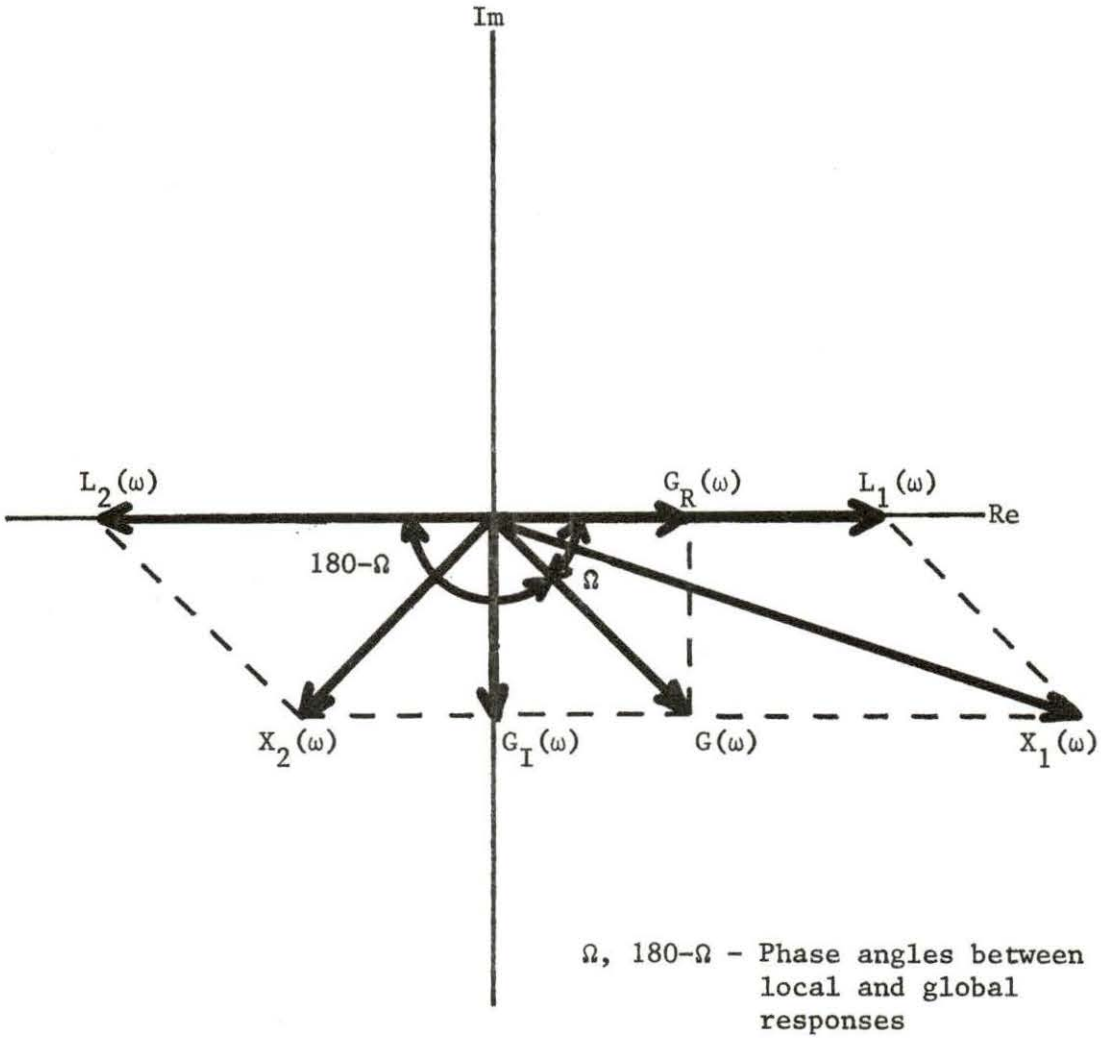

Figure 3.4. Vector representation of the local and global effects for the special one-dimensional case

Since the local effect adds for one detector while simultaneously subtracting from the other, and the global effect simultaneously affects both detectors in the same way, the detector responses in the time domain are stated as [1]

$$x_1(t) = g(t) + \ell(t) \tag{3.12}$$

$$x_2(t) = g(t) - \ell(t),$$

where the subscripts denote detectors 1 and 2, respectively.

The frequency domain responses are [1]

$$X_1(\omega) = G_R(\omega) - jG_I(\omega) + L(\omega)$$

$$X_2(\omega) = G_R(\omega) - jG_I(\omega) - L(\omega), \tag{3.13}$$

where G_R is the real global component, G_I is the imaginary global component, and L is the local component.

From the definition of the auto-power spectral density (APSD) [12],

$$APSD_1(\omega) = X_1X_1^* = (G_R+L)^2 + G_I^2$$

$$APSD_2(\omega) = X_2X_2^* = (G_R-L)^2 + G_I^2. \tag{3.14}$$

The cross-power spectral density (CPSD) may be calculated in a similar manner [13], yielding

$$CPSD_{1,2} = X_1 X_2^* = G_R^2 + G_I^2 - L^2 + j(2LG_I). \tag{3.15}$$

For the special two-dimensional case (Figures 3.2 and 3.3), both detectors have the same response and, consequently, the same signal characteristics. Thus,

$$x_1(t) = x_2(t) = g(t) + \ell(t). \tag{3.16}$$

Consequently, both detectors will have the same APSD and the CPSD will be the APSD for either detector.

2. Calculation of local-to-global ratios

The local-to-global ratio for a given detector can be a useful indicator of the proximity of that detector to the vibrating abosrber. Since the local effect is space-dependent and falls off as distance from the vibrating absorber increases, the local-to-global ratio should also decrease as distance from the absorber increases [5].

For the special one-dimensional case (Figure 3.1), the local-to-global ratio is closely related to the phase angle of the CPSD between the two detectors. This angle is

$$\Theta = \tan^{-1}\left[\frac{2LG_I}{G_R^2 + G_I^2 - L^2}\right]; \; -180^\circ < \Theta < 0^\circ. \tag{3.17}$$

From Equation (3.17), it can be seen that if the local effect tends to zero, as is the case when the distance between the detector and the vibrating absorber becomes large, the phase angle will also

tend to zero. As the detectors are moved closer to the vibrating absorber, the local effect will become more and more dominant, and the two detector signals will become more and more out of phase, with the phase angle approaching -180^{o} as the distance from the absorber approaches zero.

The local-to-global ratio may be defined as [1]

$$R_{L,G} = \frac{L}{\sqrt{G_R^2 + G_I^2}} \quad . \tag{3.18}$$

Direct inspection of Equation (3.17) shows there is no way in which the local-to-global ratio may be calculated from the CPSD phase. However, as will be shown, the CPSD phase is still useful in determining the local-to-global ratio.

Since the global component is the zero-power reactor transfer function [1], the real and imaginary global components are actually the real and imaginary parts of the reactor transfer function, which is [14]

$$G(j\omega) = \frac{n_o}{\Lambda} \cdot \frac{j\omega + \lambda}{j\omega(j\omega+\beta/\Lambda)} \quad . \tag{3.19}$$

Calculations using Equation (3.19) and parameters measured for the UTR-10 reactor [15] show that at low frequencies (0.10 Hz < ω < 2.0 Hz), the imaginary global component, G_I, becomes

very small with respect to G_R. If the G_I term is neglected in Equation (3.18), the local-to-global ratio is then

$$R_{L,G} = \frac{L}{\sqrt{G_R^2}} = \frac{L}{G_R}. \tag{3.20}$$

If the same assumption is applied to Equation (3.14), the result is

$$\begin{aligned} APSD_1 &= (G_R + L)^2 \\ APSD_2 &= (G_R - L)^2 . \end{aligned} \tag{3.21}$$

Equation (3.21) may be solved for two different ranges of the CPSD phase angle, each solution being valid only for its specific phase angle range. The solutions are

$$R_{L,G} = \frac{\sqrt{APSD_1} - \sqrt{APSD_2}}{\sqrt{APSD_1} + \sqrt{APSD_2}} ; \; -90^\circ \leq \theta < 0^\circ \tag{3.22}$$

and

$$R_{L,G} = \frac{\sqrt{APSD_1} + \sqrt{APSD_2}}{\sqrt{APSD_1} - \sqrt{APSD_2}} ; \; -180^\circ < \theta \leq -90^\circ , \tag{3.23}$$

where θ is the CPSD phase between the two detectors. Thus, a knowledge of the CPSD phase is required in determining the local-to-global ratio. An analysis of Equation (3.22) shows that it is valid

only when the local-to-global ratio is one or less, and Equation (3.23) is only useful when the ratio is one or larger. As was stated, earlier, both equations are valid only for low frequencies. Equation (3.19) shows that, as frequency increases toward $\omega=\beta/\Lambda$, the magnitude of the imaginary global component will increase, causing the local-to-global ratio to decrease slightly. At frequencies above $\omega=\beta/\Lambda$, the global effect, being the zero-power reactor transfer function, will fall off considerably [14], pushing the local-to-global ratio higher and higher as frequency increases.

For the special two-dimensional case with symmetrical detectors perpendicular to the vibration (see Figure 3.2), the situation is somewhat different since both detectors see the same perturbation and there are different frequencies involved with each of the local and global effects. However, if the vibrator can be made to oscillate sinusoidally with a frequency of $\omega=\omega_o$, Equation (3.9) shows that the reactor will also respond sinusoidally with the same frequency. However, as shown in Figure 3.3, the detectors see a local response occurring at a frequency of $\omega=2\omega_o$. The total response, as seen by the detectors, may be modeled in the time domain as

$$x(t) = g(t) + \ell(t) = g \sin(\omega_o t) + \ell \sin(2\omega_o t - \pi/2), \qquad (3.24)$$

where g and ℓ are the global and local effect magnitudes, respectively.

Therefore,

$$R_{L,G} = \frac{\ell}{g}. \tag{3.25}$$

The APSDs for each of the local and global effects are [12]

$$APSD_{\ell} = \frac{\ell^2}{2} \delta(\omega-2\omega_o) \tag{3.26}$$

and

$$APSD_g = \frac{g^2}{2} \delta(\omega-\omega_o), \tag{3.27}$$

where $APSD_{\ell}$ and $APSD_g$ are the local and global APSDs, respectively, and δ refers to the Dirac delta function.

Figure 3.5 shows how the power spectrum for this model should appear. The global and local peaks do not appear with exactly zero width at ω_o and $2\omega_o$. Therefore, it is necessary to integrate over the peak width and then subtract away the background noise integral calculated from the same bandwidth. If these operations are performed on Equations (3.26) and (3.27), the results are

$$\frac{g^2}{2} = \int_{\omega_o-\varepsilon_g}^{\omega_o+\varepsilon_g} (APSD_g - N_g)d\omega \tag{3.28}$$

and

$$\frac{\ell^2}{2} = \int_{2\omega_o-\varepsilon_{\ell}}^{2\omega_o+\varepsilon_{\ell}} (APSD_{\ell} - N_{\ell})d\omega, \tag{3.29}$$

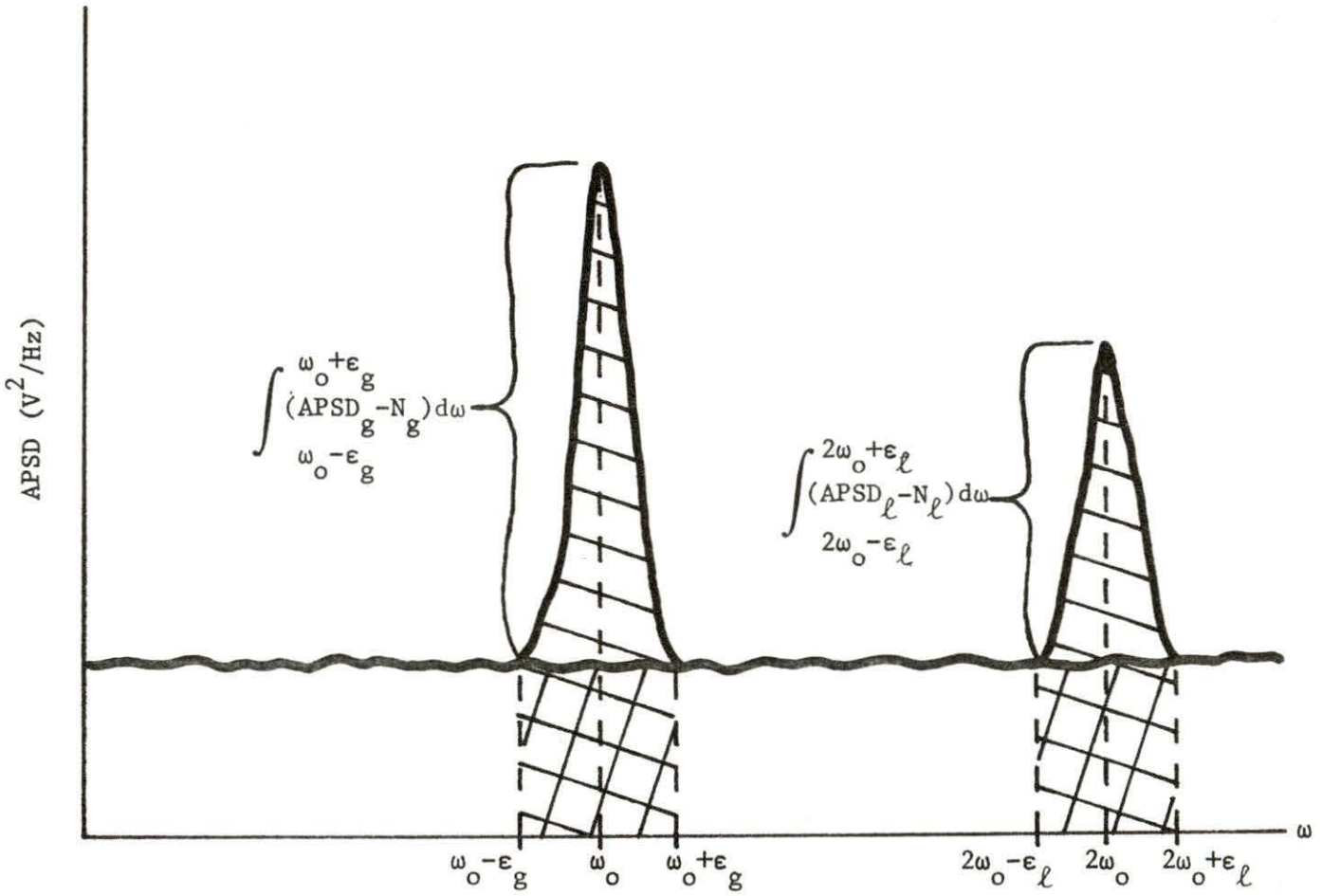

Figure 3.5. Typical power spectrum for the special two-dimensional case

where ε_g and ε_ℓ are the half-widths of the global and local peaks, respectively.

Equations (3.28) and (3.29) are solved for g and ℓ, respectively, and the results are then substituted into Equation (3.25). Thus, the local-to-global ratio for the special two-dimensional case is

$$R_{L,G} = \frac{\sqrt{\int_{2\omega_o-\varepsilon_\ell}^{2\omega_o+\varepsilon_\ell} (APSD_\ell - N_\ell)\, d\omega}}{\sqrt{\int_{\omega_o-\varepsilon_g}^{\omega_o+\varepsilon_g} (APSD_g - N_g)\, d\omega}} \quad . \tag{3.30}$$

IV. EXPERIMENTAL APPARATUS AND PROCEDURES

A. Experimental Apparatus

1. The UTR-10 reactor

The UTR-10 [16] is an Argonaut-type 10 kilowatt, light-water moderated and cooled, graphite-reflected reactor. The reactor core consists of two parallel rectangular core tanks separated by 46 centimeters of graphite. The core tanks are surrounded by a graphite reflector 142 centimeters long, 112 centimeters wide and 122 centimeters deep. Each core tank holds six fuel assemblies with each assembly containing up to twelve fuel plates. The fuel plates are composed of an aluminum clad surrounding an aluminum-uranium alloy, with the uranium enriched to about 93% in U-235.

Directly between the two core tanks in the center of the core region is a 122 cm x 10 cm x 10 cm removable central vertical stringer (CVS). For this experiment, the CVS was removed and the experimental apparatus was inserted in its place. The thermal flux at the mid-elevation in the CVS is approximately 10^7 neutrons/cm^2-sec per watt of reactor power.

Figures 4.1 and 4.2 show two different views of the reactor configuration.

2. The vibrating absorber assembly

The vibrating absorber assembly consisted of an aluminum box, which contained the drive mechanism for the vibrating absorber,

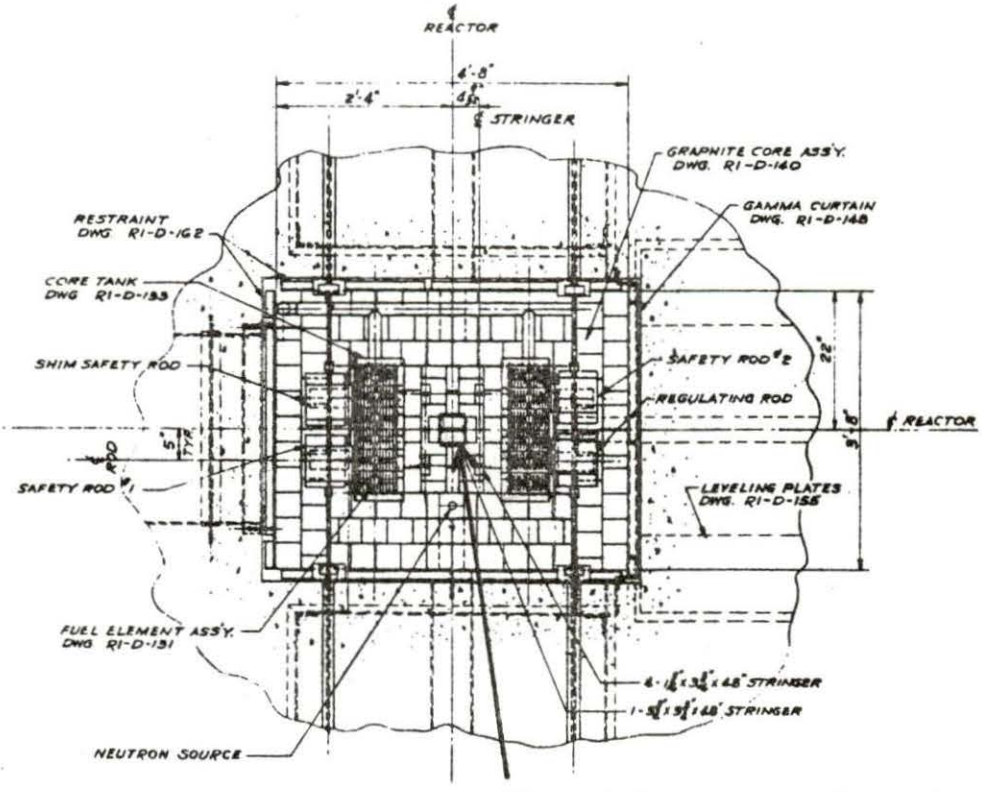

Central Vertical Stringer (CVS)

Figure 4.1. Top view of UTR-10 core area showing location of central vertical stringer

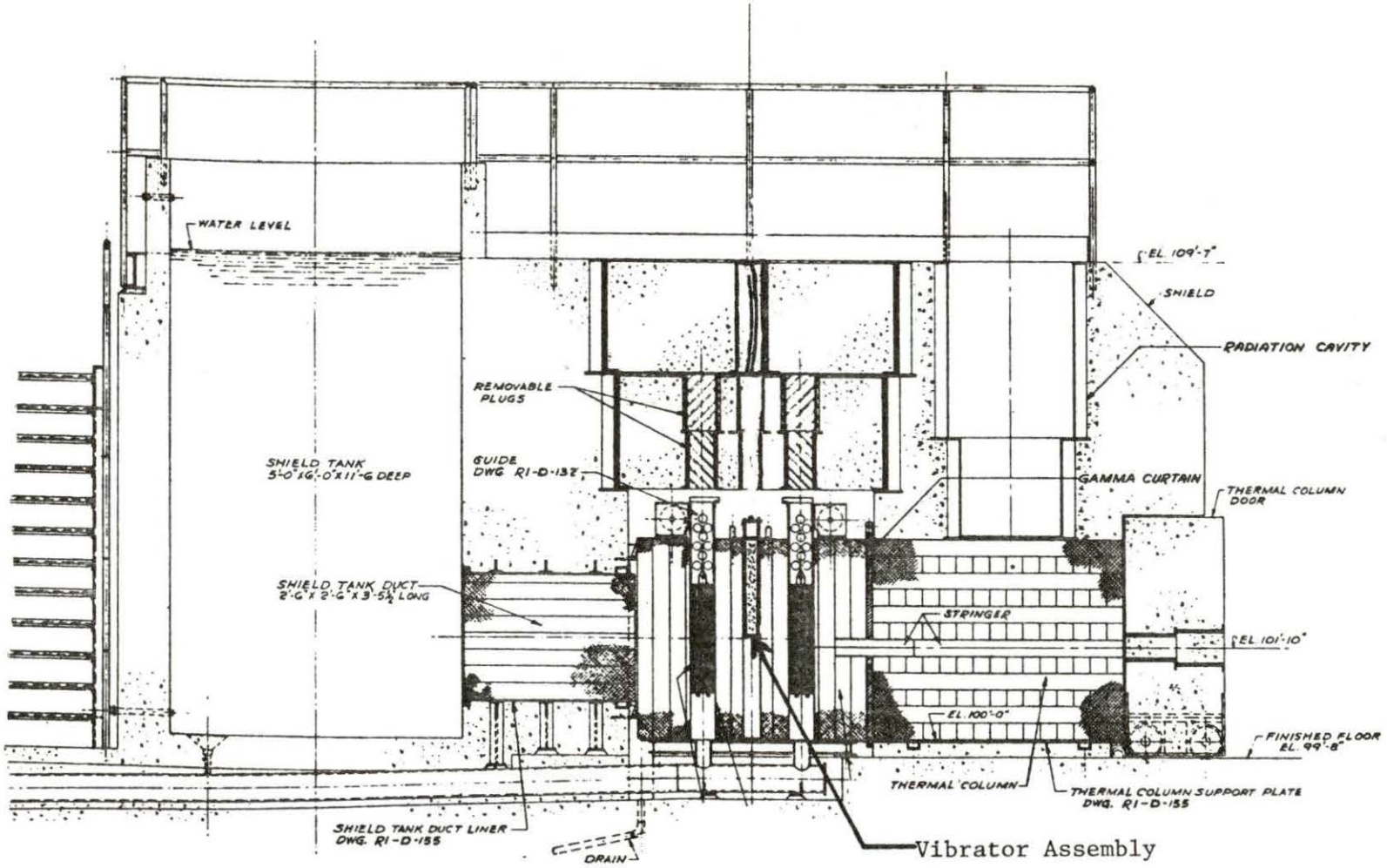

Figure 4.2. Longitudinal cross section of the UTR-10 showing location of the vibrator in core

and two specially machined graphite slabs that, when fitted together, would fit into the space created by the removal of the CVS. The graphite slabs, shown in Figure 4.3, had three machined channels; one channel to house the vibrating absorber, and two channels that each held a BF_3 neutron detector. The aluminum box, 10.2 cm x 10.2 cm x 12.7 cm, was secured to the top of the graphite slabs. The box contained two 28 volt, 0.3 ampere DC coils for driving the vibrating absorber and a linear variable differential transformer (LVDT) for measuring the position of the vibrating absorber.

The vibrating absorber consisted of a 5 cm x 2 cm x 0.025 cm strip of cadmium metal that was secured with steel mounting screws into a 5 cm slot cut into one end of a 68.3 cm long by 0.6 cm diameter aluminum rod. At the other end of the rod, an aluminum block, 2.5 cm x 2.5 cm x 1.3 cm, with iron plates cemented to its sides, was attached to the rod. By placing the two DC coils on either side of the block and charging them alternately to generate magnetic fields, the rod was made to pivot back and forth about a steel pin, thus creating a vibrating motion with a maximum amplitude of 1.28 cm for the cadmium absorber. The movement of the cadmium absorber created fluctuations in the neutron field in the reactor which were detected by the two BF_3 neutron detectors. Figure 4.4 shows the basic components of this setup.

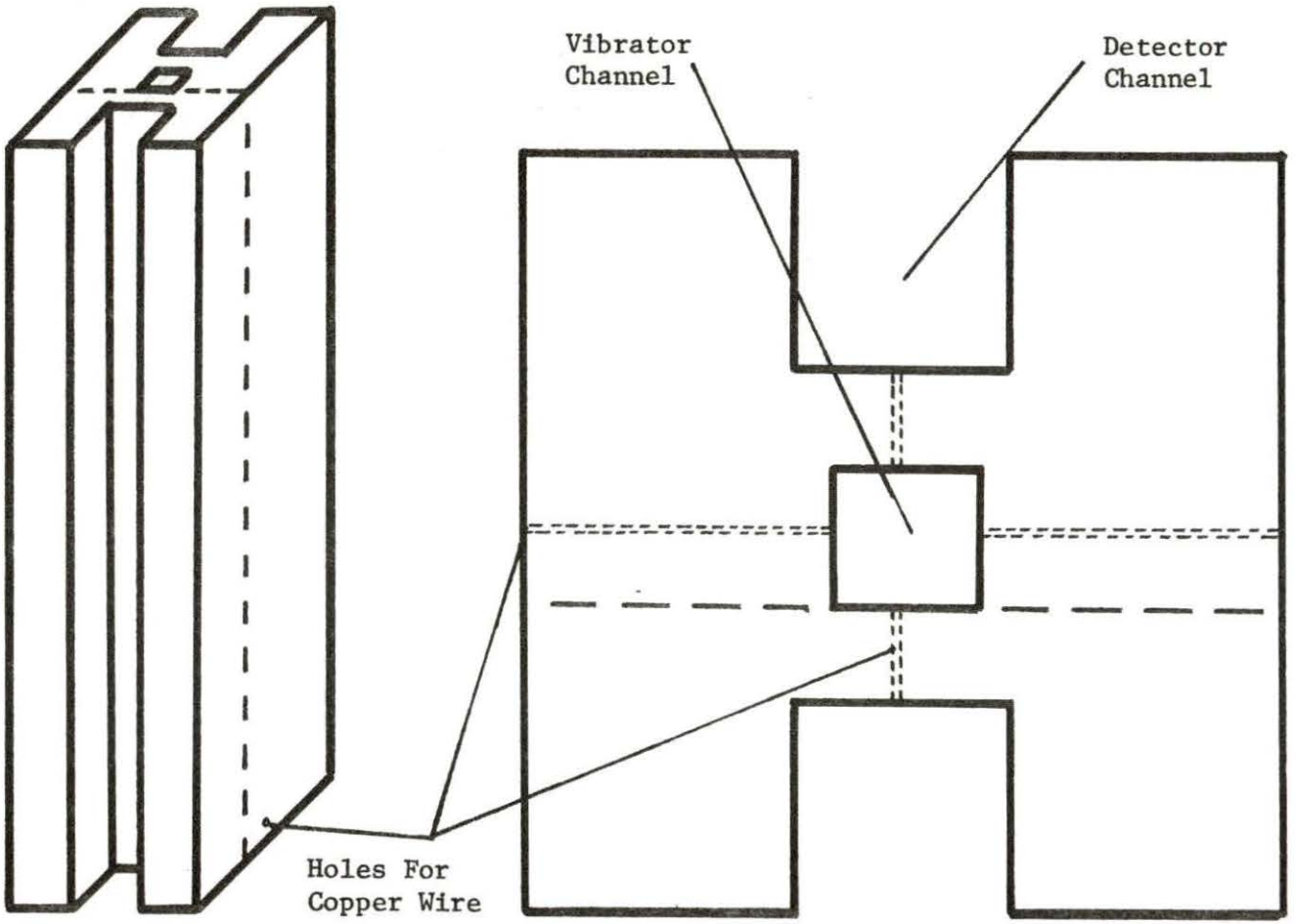

Figure 4.3. Graphite slabs for vibrator apparatus

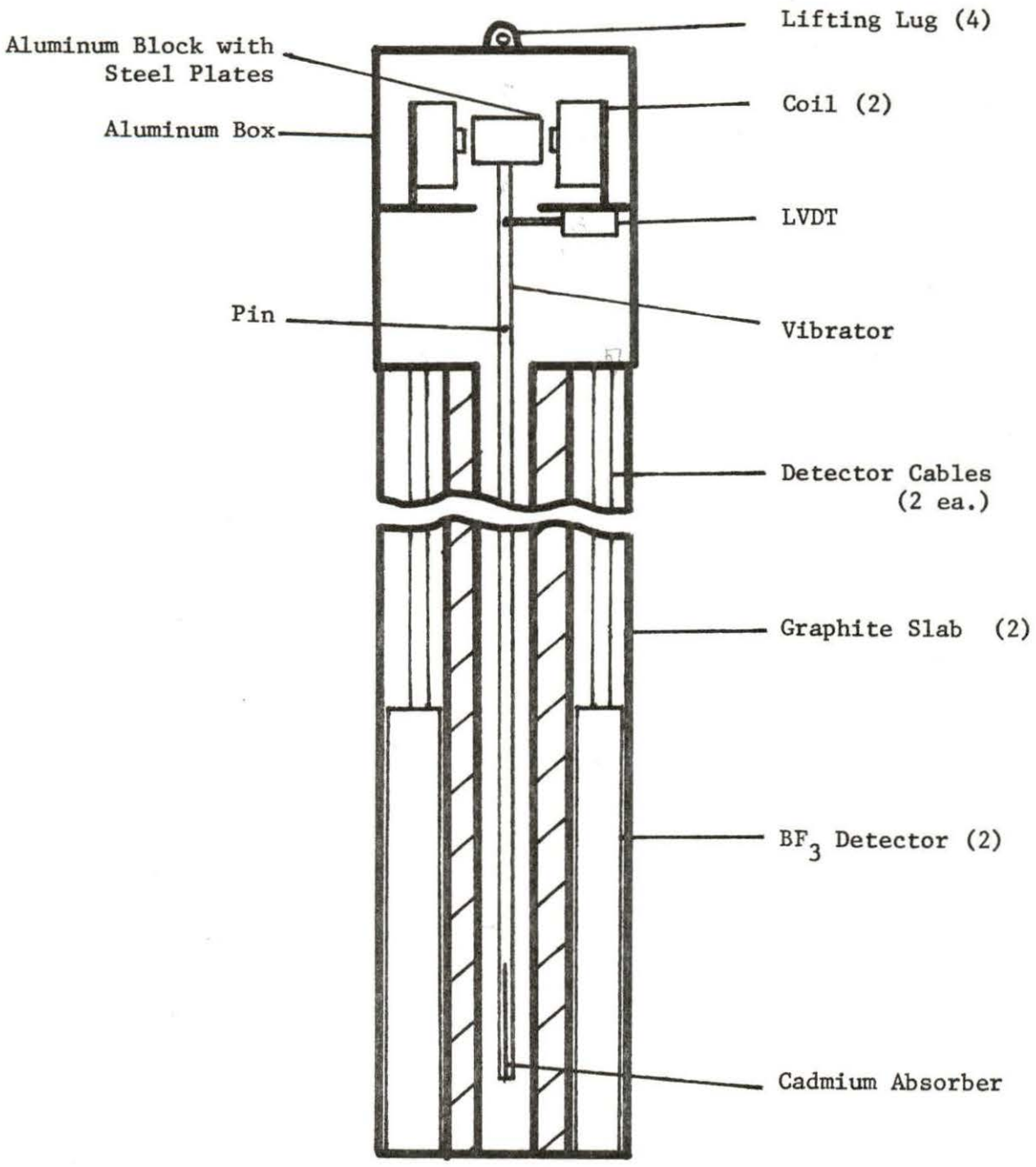

Figure 4.4. Internal mechanisms of the vibrator apparatus

The coil driving system is shown in Figure 4.5. Two types of driving signals were used; a square wave from a signal generator (Wavetek Model 111) and a pseudo-random binary sequence (PRBS) from a noise generator (Hewlett Packard Model 3722 A). The signals from these generators were used to drive an electronic switching circuit constructed by the ISU Engineering Research Institute (ERI) Electronics Shop. This circuit would switch power from a variable DC voltage supply back and forth between the two coils, causing the absorber to vibrate. The coils themselves were surrounded by magnetic shielding material to help reduce the unwanted electronic noise that the oscillating magnetic fields were inducing in the various data channels.

The linear variable differential transformer (Schaevitz Engineering Model 100 MHR) was a hollow cylindrical transformer with a movable core. Magnetic field end effects generated by the movement of the core were detected by the transformer coils and were converted into a modulated signal whose amplitude was directly and linearly proportional to the position of the core relative to the transformer coils. An external electronics package provided the modulating signal required by the primary LVDT coil and also demodulated the output from the secondary LVDT coils into a simple DC voltage [17]. By attaching the core to the vibrating aluminum rod with two short pieces of threaded steel rod, the position of

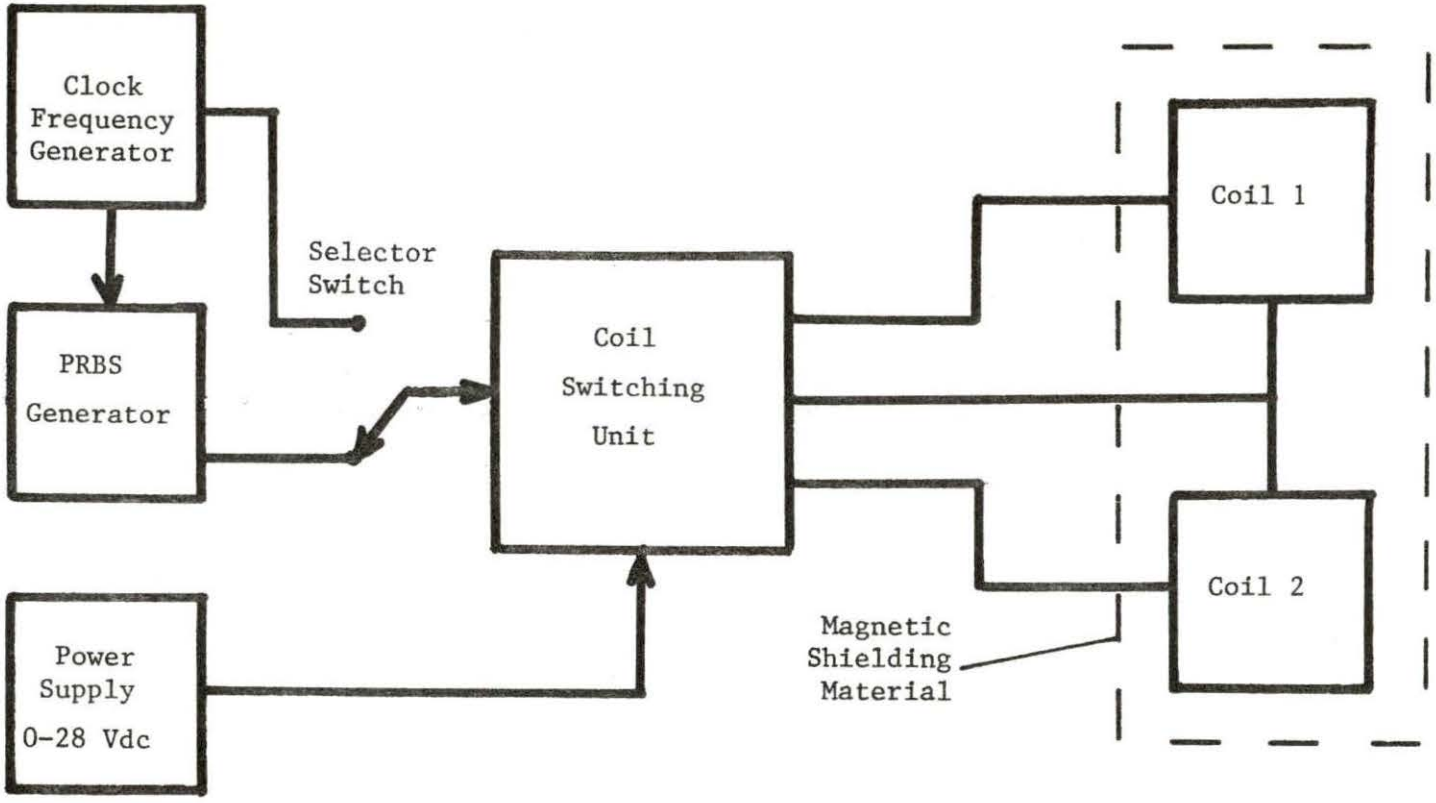

Figure 4.5. Block diagram of magnetic coil driving system

the vibrating absorber was monitored by observing the DC output voltage from the electronics package. A schematic diagram of this hookup is shown in Figure 4.6.

In order to monitor the neutron flux fluctuations created by the vibrating absorber, two BF_3 neutron detectors (N. Wood Counter Laboratory Model G-10-2A, 120 cm Hg gas pressure) were used. The detectors were operated in the ion chamber mode with a battery-supplied operating voltage of 270 volts. With the detector center wire connected to the negative side of the circuit and the detector casing hooked to the positive side, the circuit would produce a current that was proportional to the neutron flux in the detector. The detectors were covered with layers of plastic and aluminum foil to protect them from short circuits and unwanted electronic noise. The detector cables were also shielded by copper braids. A more detailed analysis of the unwanted electromagnetic noise problem and the measures taken to counteract it is presented in Appendix B.

B. Signal Processing and Data Analysis

1. Signal processing

There were three different signal channels available for processing and analysis: one channel of flux information from each of the two detectors and one channel of absorber position data from the LVDT.

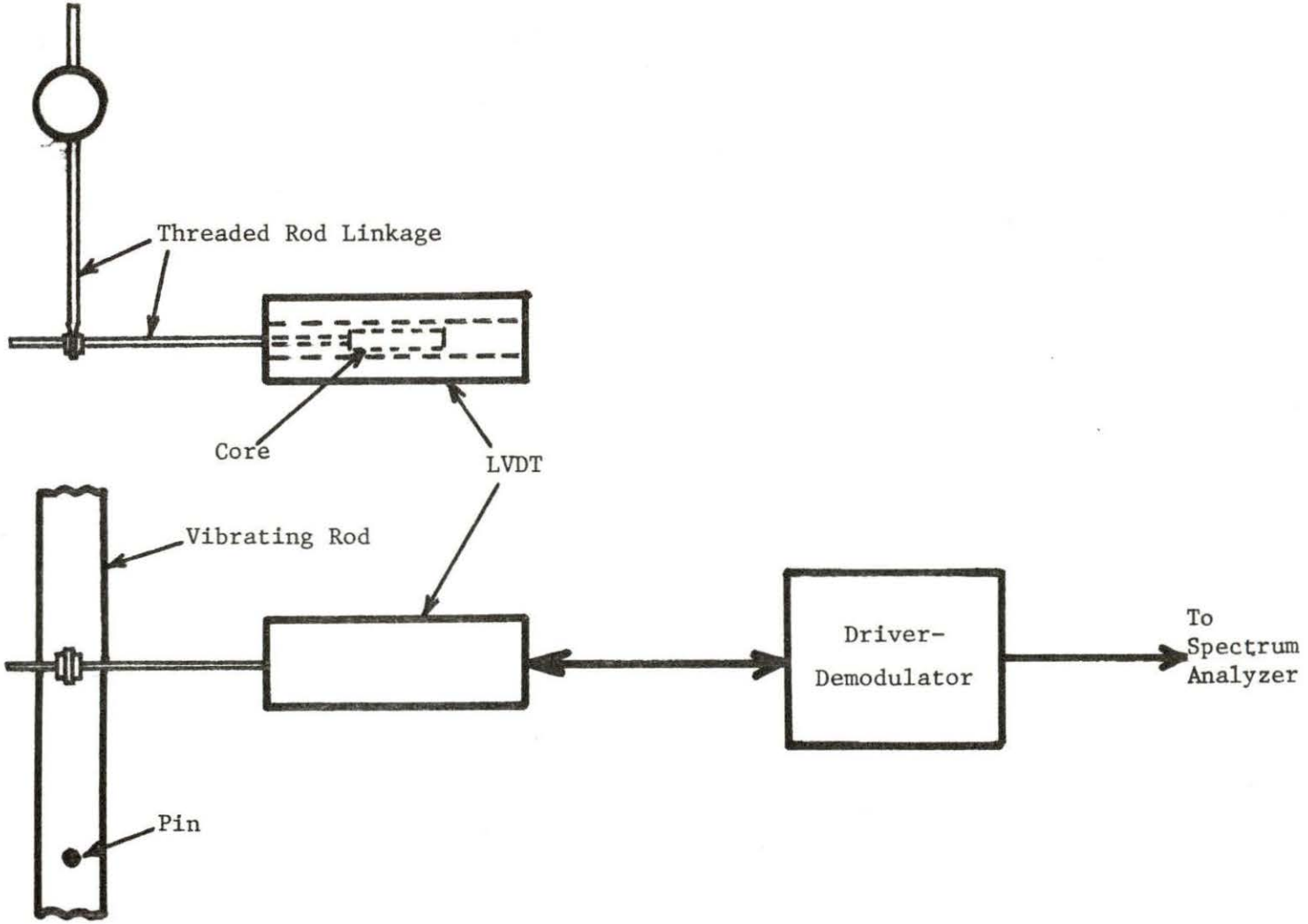

Figure 4.6. Block diagram of vibrator position measuring system

As seen in Figure 4.7, the current output of each detector was fed into a preamplifier (Ames Laboratory Electronics Model 1616), which acted as a current-to-voltage converter. The voltage signal from each preamp was then fed into a second-order Butterworth high-pass filter (Burr-Brown Model UAF 11) that had a cutoff frequency of 0.097 Hertz. This filter eliminated the DC component of the detector signal, leaving only the noise component.

The detector noise signals were then fed into a fourth-order Butterworth low-pass filter (Krohn-Hite Model 3321). This filter, with its cutoff set at 12.0 Hertz, eliminated unwanted high frequency noise from the detector signals, particularly 60 Hertz noise from other electrical equipment operating in the vicinity.

As shown in Figures 4.6 and 4.7, the detector and LVDT signals were then fed into a two-channel frequency spectrum analyzer (Hewlett Packard Model 3582A). When used in the dual channel mode, the spectrum analyzer not only calculated single-channel frequency spectra, but could also be used to calculate the transfer function magnitude and phase between the two channels. By using different combinations of the three data channels as inputs to the analyzer, it was possible to obtain a wide variety of frequency spectra and transfer functions, which could be used in later calculations.

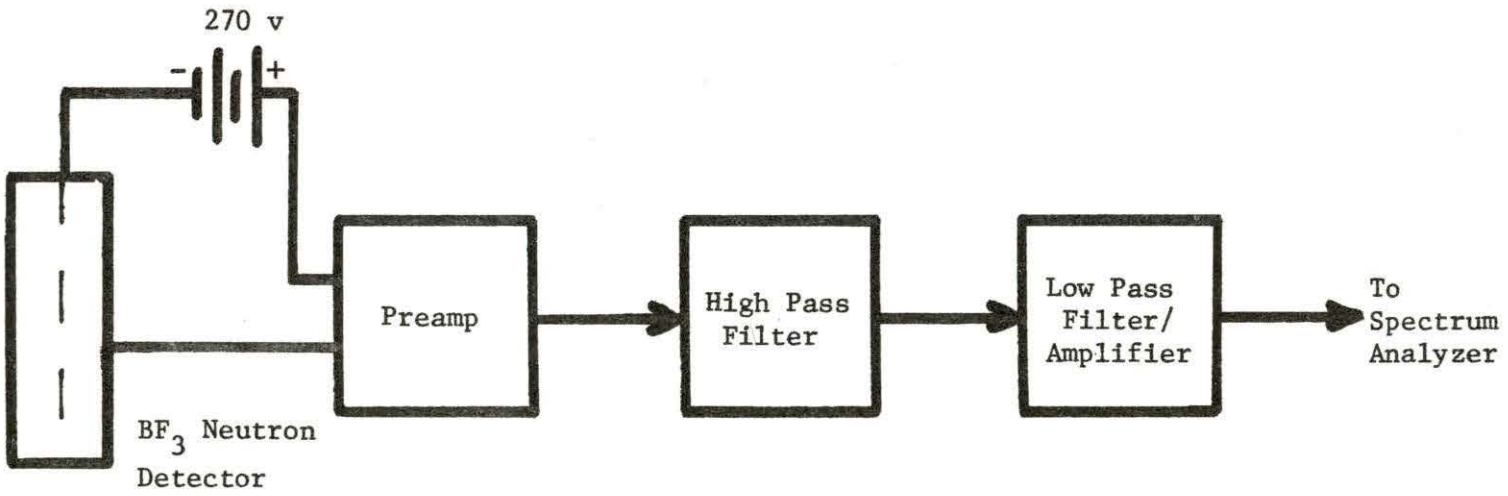

Figure 4.7. Block diagram of the neutron noise measuring system

2. Computer data analysis

The spectrum analyzer interfaced with a Hewlett Packard Model 85 microcomputer. Various programs were developed for this computer that allowed the user to perform manipulations with the data from the spectrum analyzer. Figure 4.8 shows the hierarchy of the computer programs and how they interact with each other and the spectrum analyzer.

The program DATSTR was used to store spectral magnitude and phase data from the spectrum analyzer on a floppy disk for later use. The program APSD was used to calculate and store auto-power spectral densities from single channel spectral data stored by DATSTR. The program CPSD calculated and stored cross-power spectral density magnitudes from auto-power spectral density data stored by APSD and from transfer function magnitude data obtained from the spectrum analyzer using DATSTR. The program LGRAT used APSD data to calculate local-to-global ratios. The program could use either Equation (3.22), (3.23), or (3.30) to perform the calculation, the selection being dependent upon the experimental mode.

The codes PLOT5 and PHASE were used to plot spectral magnitudes and phases, respectively, using a Hewlett-Packard Model 7225A plotter.

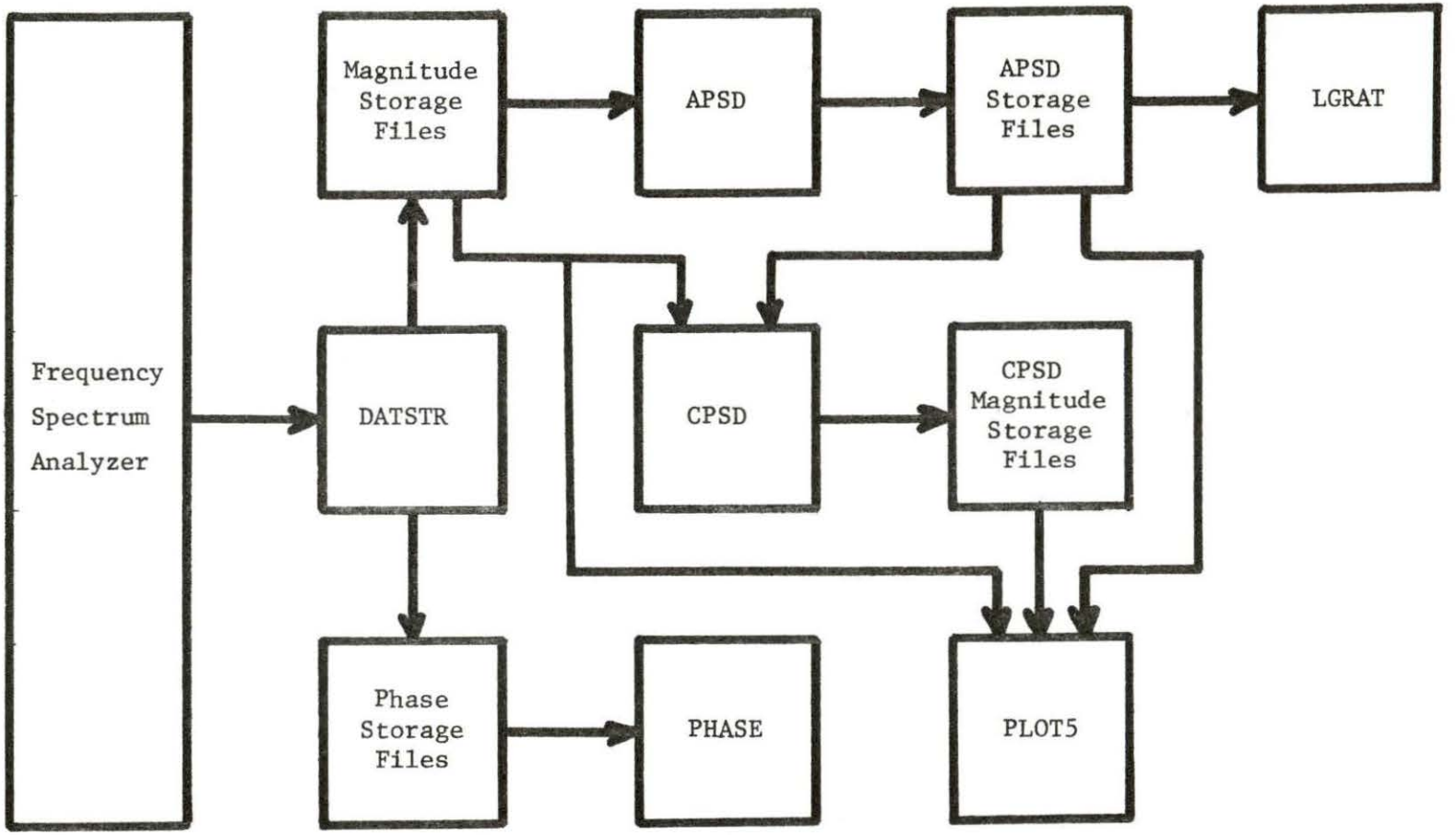

Figure 4.8. Block diagram of the computer code interactions

C. Experimental Procedures

1. Experimental modes

The vibrating absorber apparatus was constructed in such a way that the motion of the vibrating absorber could be rotated by ninety degrees with respect to the detectors. Thus, measurements could be taken with the vibrating absorber moving in line with the detectors or with the absorber moving perpendicular to the detector line. In addition, the entire apparatus could be rotated by ninety degrees with respect to the reactor core tanks. Thus, by combining the two types of rotations, four different experimental modes were possible. These modes are shown schematically in Figure 4.9.

In order to conveniently designate the different experimental modes, each mode was assigned a four letter designation which described the vibrating absorber motion and the detector positions. The first two letters indicated the direction of the absorber motion and the last two letters specified the position of the detectors. For example, the experimental mode shown in Figure 4.9d pictures the vibrating absorber moving in an East-West direction and the detectors located to the North and South of the absorber. Therefore, the designation for this mode is EWNS.

As was stated earlier, modes NSNS and EWEW had been examined previously [1,9], but modes NSEW and EWNS had not been examined.

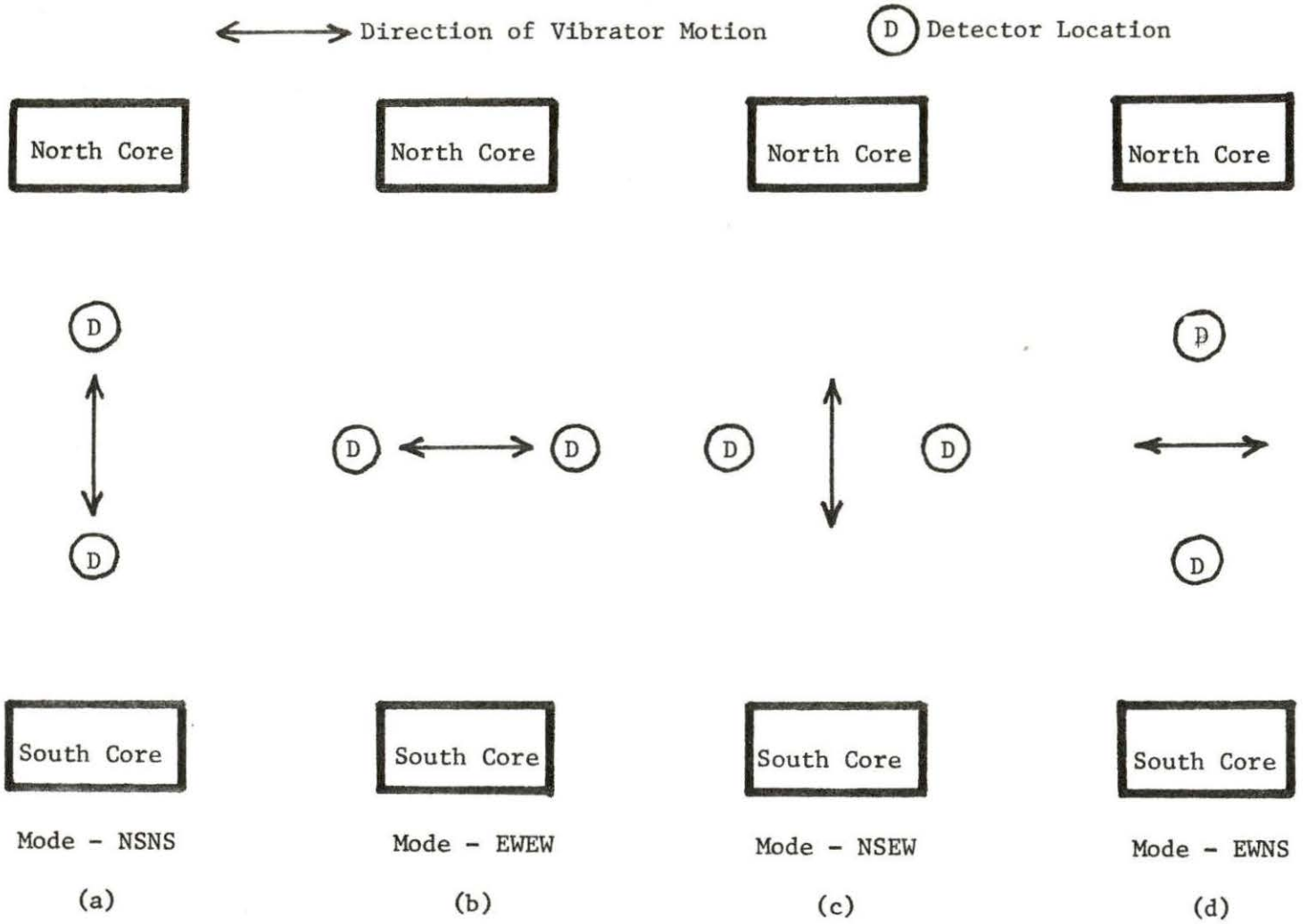

Figure 4.9. Schematic representation of the experimental modes

2. Vibrating absorber drive modes

It was determined that for the NSNS and EWEW modes, it would be advantageous to use a PRBS driving signal for the coils, since it would generate a complete, continuous spectrum of input frequencies, as opposed to a spectrum of discrete points that would be produced by a single-frequency square wave input. The local-to-global ratio could be calculated by using Equation (3.22) or (3.23) and the discrete APSD data points calculated from the spectrum analyzer data.

The NSEW and EWNS modes were identical to the special cases illustrated in Figure 3.3. In order to use Equation (3.30) to calculate the local-to-global ratio for these modes, the absorber had to move in such a manner that it did not generate a harmonic at two times the fundamental frequency. If such a harmonic was present in the absorber motion specturm, the global response could possibly mix with or mask the local response (see Figure 3.5). Ideally, a sinusoidal motion was best since it contains no harmonics. However, the manner in which the vibrator was driven did not allow the vibrator to move in a sinusoidal fashion. The absorber could, however, be made to move in a square-wave motion, and since a square wave has no harmonic at two times its fundamental frequency, no mixing or masking effects would be expected to occur.

3. Vibrator testing

In order to test the performance of the apparatus and vibrator driving system, a PRBS signal was used to drive the coils. The transfer function between the PRBS input and the vibrating absorber position, as measured by the LVDT, was calculated using the spectrum analyzer. The phase of that transfer function is shown in Figure 4.10 for the frequency range of 0 to 10 Hertz. As might be expected, the vibrating absorber began to lag behind the system input at higher frequencies. This effect was due to the inertia of the vibrating absorber. The absorber was observed to have a resonant frequency if the LVDT output was examined on an oscilloscope. The resonant frequency was not in the range of 0 to 10 Hertz and, therefore, the spectrum analyzer had to be reset to observe a larger frequency range. An examination of the PRBS input - LVDT output transfer function magnitude, shown in Figure 4.11, revealed that the resonant frequency of the vibrating absorber was 13.8 Hertz, which was well above the frequency range of interest and, therefore, had no effect on the measurements that were made in that range.

The spectral characteristics of the vibrating absorber were determined by analyzing the LVDT output with the spectrum analyzer and then using the computer to calculate the APSD for each particular

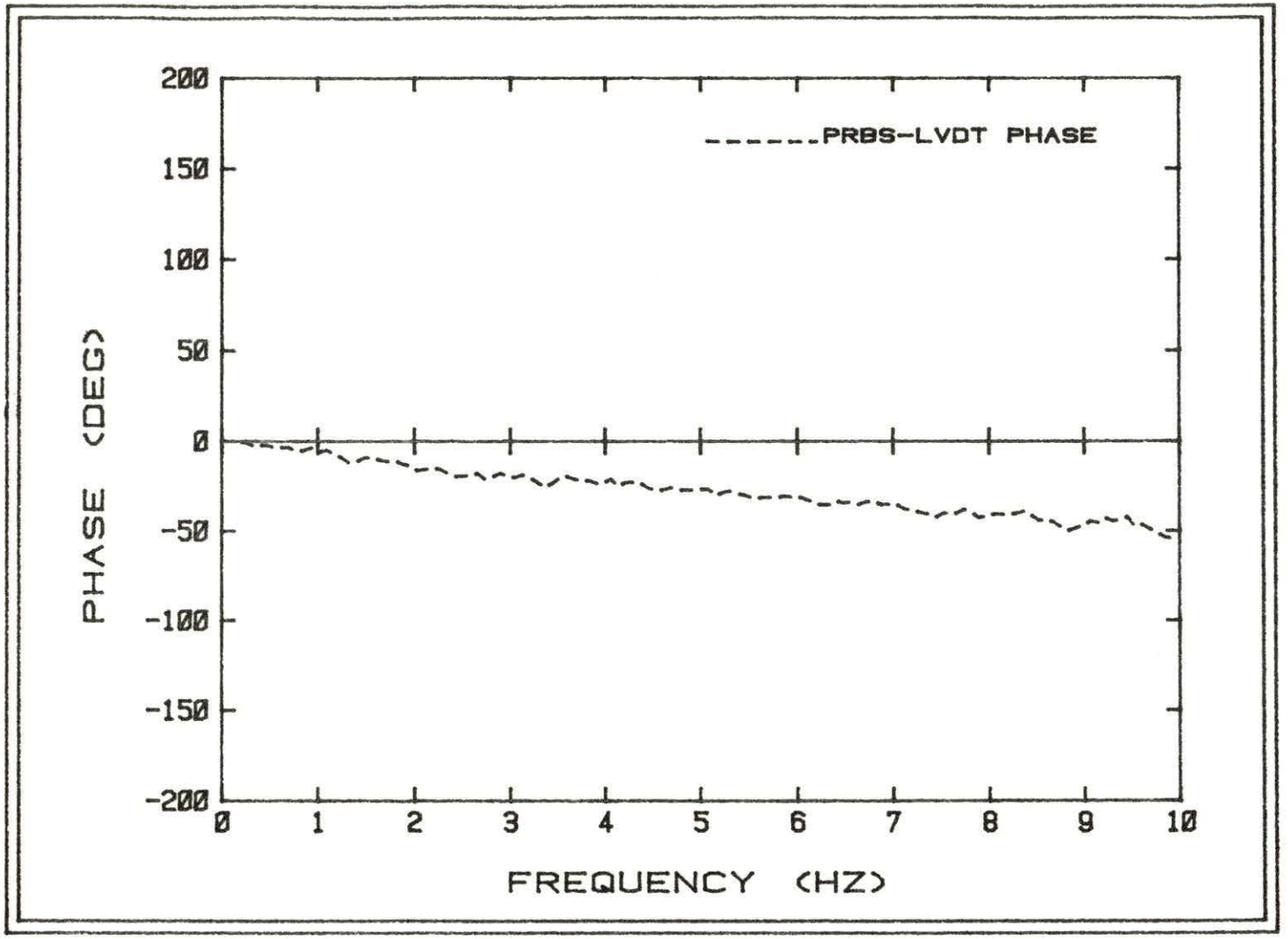

Figure 4.10. Transfer function phase between PRBS input and LVDT output

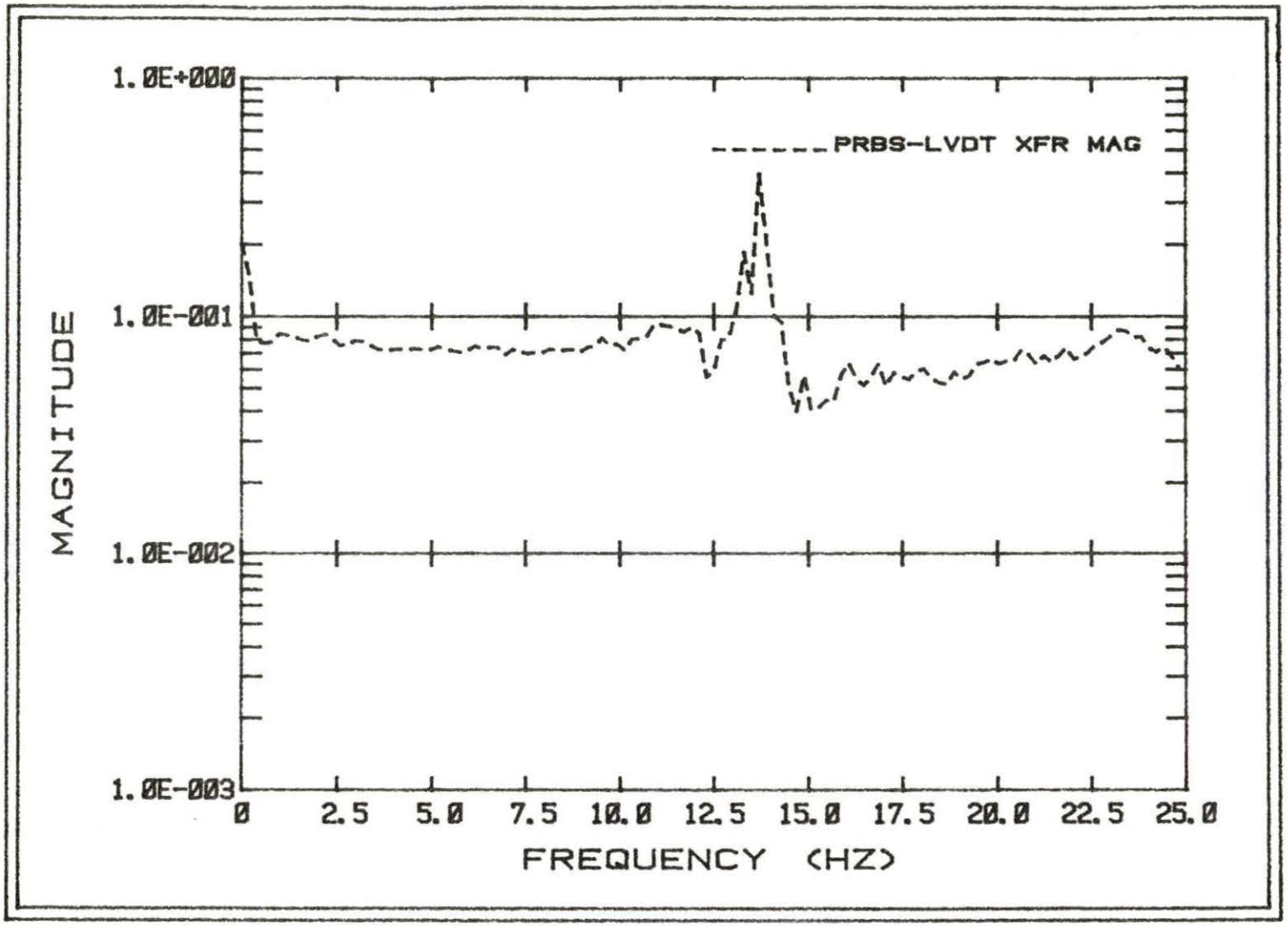

Figure 4.11. Transfer function magnitude between PRBS input and LVDT output

input mode. Figure 4.12 shows the APSD of the absorber motion for a PRBS input with a clock frequency of 12.0 Hertz, and Figure 4.13 illustrates the APSD for square wave input frequencies of 1.0 Hertz and 3.7 Hertz. As Figure 4.13, there is no harmonic at two times the fundamental frequency that is within two orders of magnitude of the fundamental peak. Thus, any frequency component of the input that might exist there would have virtually no mixing or masking effects on the reactor response.

An interesting phenomenon was noticed when the transfer function phase between the LVDT signal and the detector signals was examined for a PRBS input motion. Figure 4.14 shows these phase angles. It can be seen that at low frequencies, the detector response actually leads the vibrating absorber motion, A close visual examination of the absorber motion showed that the bottom of the vibrator struck the side of the graphite slabs before the iron plates at the top of the vibrator made contact with the magnetic coils. Consequently, the vibrator was slightly flexed when both the top and the bottom of it were in contact with the coils and the slabs, respectively. When the coil released the top of the vibrator, the bottom was already out ahead of the top. The detector response depends mostly on the position of the bottom of the vibrator, since that is where the cadmium strip is, whereas the LVDT measures the vibrator position at the top. Therefore, the detector response would be expected to lead the vibrator motion.

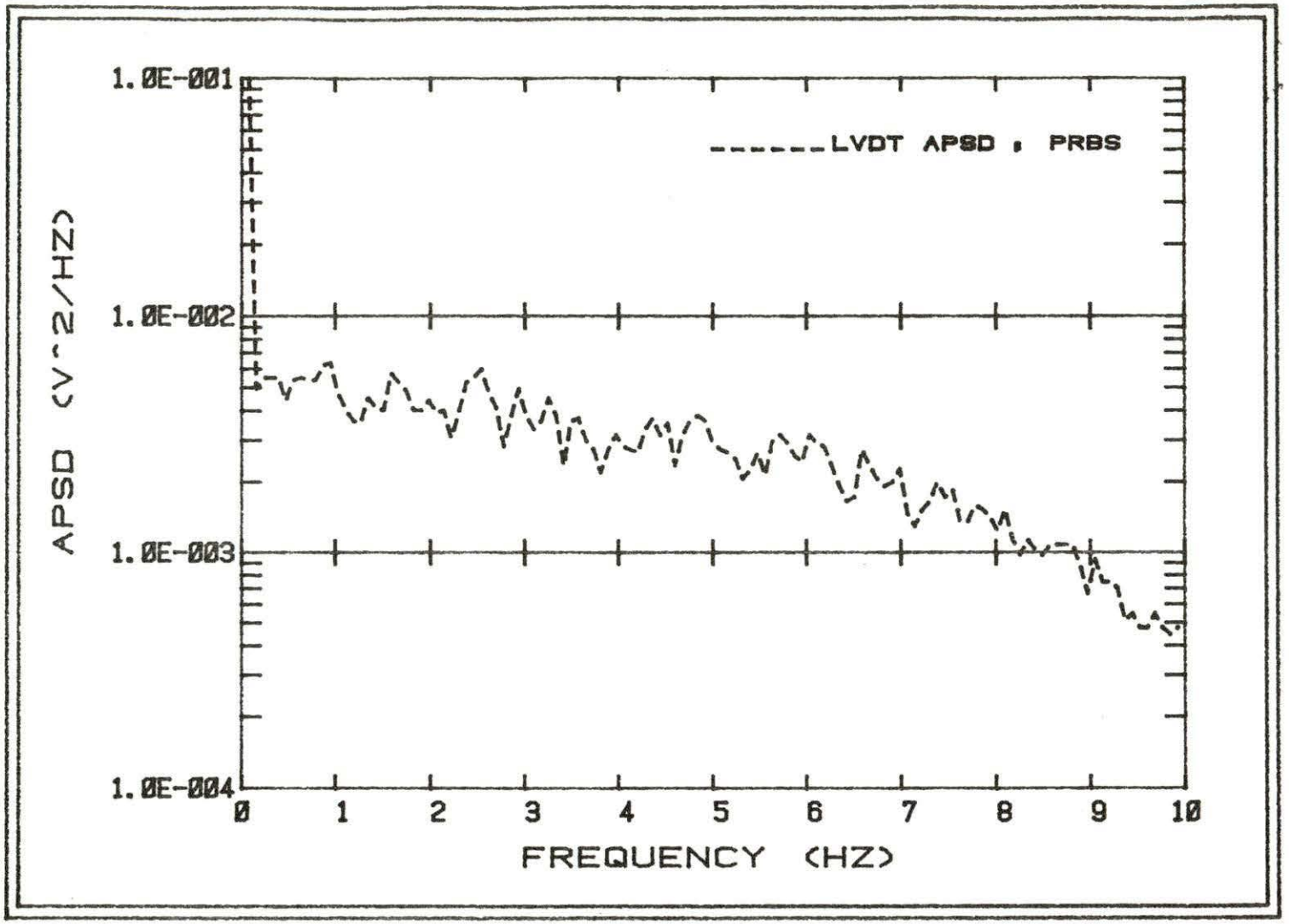

Figure 4.12. Auto-power spectral density of vibrating absorber motion for PRBS input

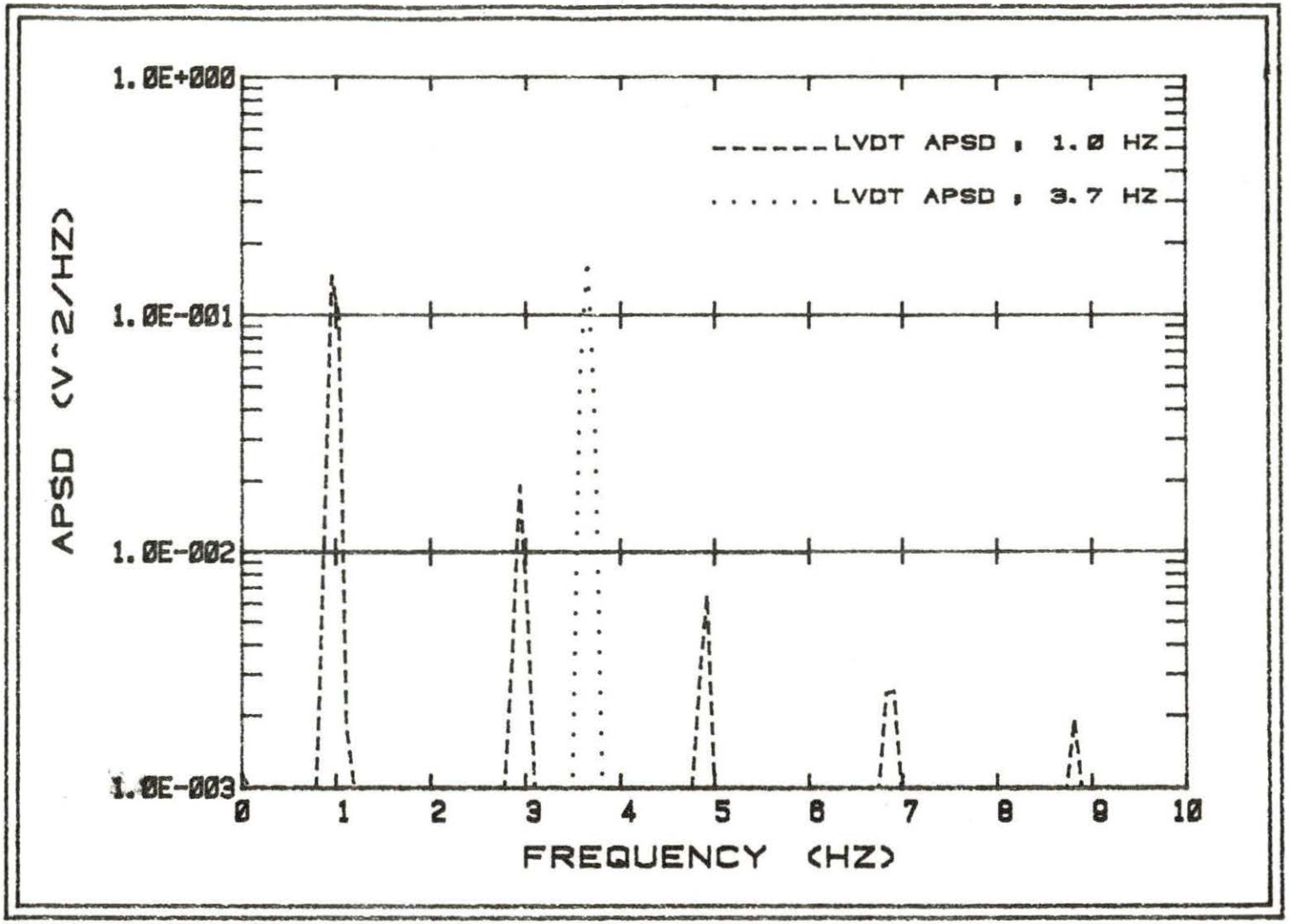

Figure 4.13. Auto-power spectral densities of vibrating absorber motion for square wave inputs

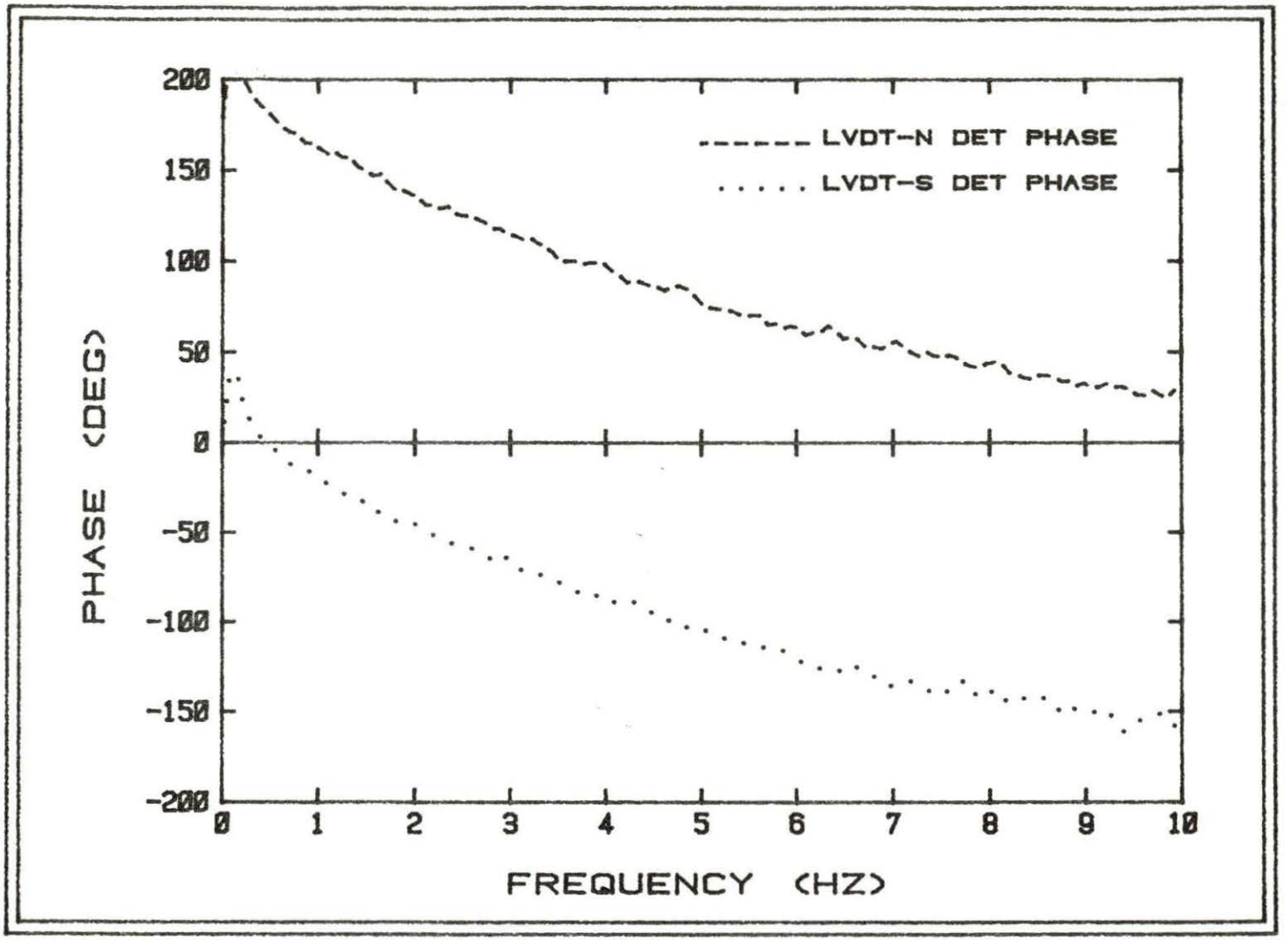

Figure 4.14. Transfer function phases between vibrator position and detector signals for PRBS input

The large phase shift of almost 150 degrees between the LVDT and the detectors at high frequencies is due to the bottom of the vibrator lagging behind the top at these frequencies. This "whipping" motion is due to the length and thinness of the vibrator.

4. Signal process testing

In order to compare the two detector signal channels (preamps, filters, etc.) for differences in gain and phase, a current source modulated by white noise was fed into the preamps and the transfer function magnitude and phase between the two channels were examined. After some minor adjustments, it was possible to reduce the difference in the gains in the two channels to less than one-half of one percent for any point in the frequency range of 0.16 Hertz to 10.16 Hertz. The phase difference between the two channels over the same frequency range was never more than plus or minus one degree.

5. Data normalization

In order to normalize the data, the settings on all instruments were kept constant for all reactor runs, with the exception that the input sensitivities on the spectrum analyzer were increased by a factor of 10 and the reactor power was increased by a factor of 5 for runs made in the NSEW and EWNS modes. It was found that the fluctuations in the neutron flux were much smaller when the apparatus was operated in these modes.

For all reactor runs, the shim rod was kept at 72.6% withdrawn. The static reactivity of the apparatus in the CVS was between -40.0 cents and -41.0 cents, depending upon the mode. The regulating rod position varied from 42% to 48%. The dynamic reactivity created by the moving absorber was not large enough to be detected by any of the reactor instrumentation. The reactor was operated under automatic control, which minimized power drift and had no effect on measurements of this type [1]. The reactor inlet coolant temperature was kept constant at 85^{o}F for all runs.

6. Flux gradient measurements

The response that the reactor exhibited during these experiments was highly dependent on the thermal neutron flux gradients that existed in the central vertical stringer region. Consequently, it was desirable to attempt to measure the flux gradients in the CVS. This was done by inserting high purity copper wires into small holes at the bottom of the graphite slabs (see Figure 4.3) and then irradiating the apparatus in the CVS with the absorber motionless. The wires were then cut into segments and the activity of 12.71-hour copper-64 was measured for each segment after waiting long enough for any 5.1-minute copper-66 that might be present to decay away. The activity of each segment was proportional to the neutron flux seen by that segment during the irradiation.

The activity of the copper wire segments was measured using a gas-flow proportional detector, and the program GRAD was used to calculate the relative thermal flux for each segment. The standard cadmium difference technique [18] was used to eliminate the effects of non-thermal neutrons. The cadmium ratio was calculated for each segment, and it was defined as

$$CR = \frac{A_b}{A_{Cd}}, \tag{4.1}$$

where CR was the cadmium ratio, A_b was the activity of the bare segment, and A_{Cd} was the activity of the cadmium-covered segment. The activity due solely to the thermal neutron flux was

$$A_{th} = \frac{CR-1}{CR} A_b, \tag{4.2}$$

where A_{th} was the thermal neutron flux-induced activity of the wire segment. From the thermal activities of all of the segments, the relative thermal fluxes and relative thermal flux gradients were determined.

V. EXPERIMENTAL RESULTS

In order to conduct measurements using the UTR-10 reactor, an Experiment Plan was prepared and submitted for review to the Reactor Use Committee. This plan described in detail the construction of the apparatus, the materials used, operating procedures, potential hazards, both radiological and otherwise, and the safeguards, both inherent and engineered, that minimized the hazards involved with the experiment.

In this section, the results of the many measurements are examined. In doing this, it is desirable to discuss the results of the thermal neutron flux gradient measurements first, since an estimate of the characteristics of the flux gradients is important to understanding the results of the vibrator measurements.

A. Flux Gradient Calculations

The flux gradient measurements were performed under the same conditions as the vibrator measurements with the exception that the vibrator was motionless during the irradiation.

Unfortunately, useful results in trying to measure the flux gradients with this method were not achieved. The activities of the wire segments were nearly all in the same range, and the variation in the flux gradients appears to be on the order of the measurement error.

Another problem associated with this method is that even if the measurement error were small, only a very coarse gradient measurement across the CVS is provided. In order to get a much finer gradient measurement, especially in the region of the cadmium strip, the wire would have to be cut into very small segments, perhaps a millimeter in length. This was not possible with the facilities available. For these reasons, it would be advantageous to develop a different method of measuring the thermal flux gradients.

An examination of the fuel loading pattern in the UTR-10 provided a qualitative knowledge of these gradients. Figure 5.1 shows the fuel loading pattern in terms of grams of U-235 per assembly [19], and in grams of U-235 per quarter-core. From the fuel loading pattern, the neutron flux would be expected to be highest in the northeast and lowest in the southwest. Thus, the gradients slope from the north and the east downward to the south and west. Calculations done for the UTR-10 with WHIRLAWAY [8] also indicated that these flux gradients existed; however, the gradient in the east-west plane had a smaller magnitude than that in the north-south plane due to the large amount of leakage in the east and west directions. Previous vibrator experiments performed with the same fuel loading pattern [1,9] confirmed the calculations made with WHIRLAWAY. Both calculations and measurements indicate that there should be a global response to both a north-south or an

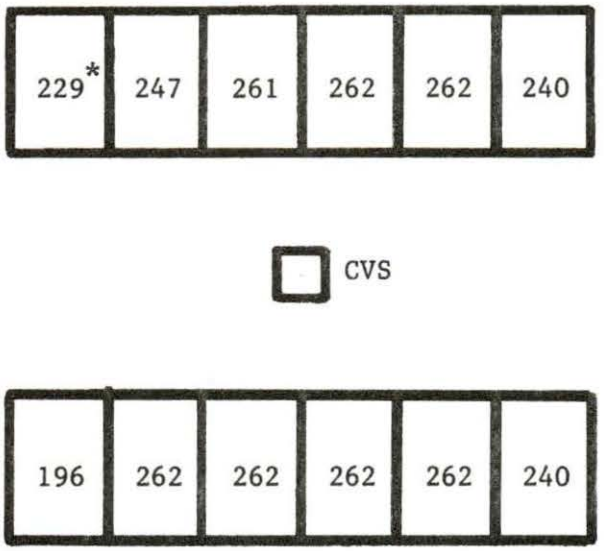

(a) by assembly

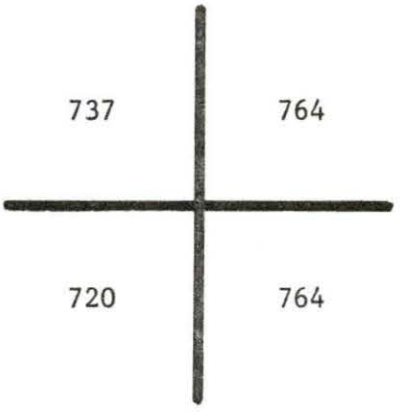

*grams of U-235

(b) by quarter-core

Figure 5.1. UTR-10 fuel loading pattern by assembly and by quarter-core

east-west movement of the absorber in the CVS, with the global response to the east-west vibration being smaller in magnitude due to the flatter flux gradient in that plane.

B. Vibrator Measurements

1. NSNS mode

Figure 5.2 shows the CPSD phase that was calculated between the two detector signals for the NSNS mode. The phase angle was very close to -180° over the entire frequency range; consequently, the local effect dominated the detector responses. Also, since the phase angle fell in the range of $-180^{\circ} < \theta \leq -90^{\circ}$, Equation (3.23) was used in calculating the local-to-global ratio.

Figure 5.3 illustrates the auto-power spectral densities of the two detector signals for a PRBS input. Their close proximity to each other indicated that either the local or the global effect dominated. Using the APSD data in the frequency range of 0.16 Hz to 2.0 Hz, LGRAT calculated an average local-to-global ratio of 15.8 over that frequency range, with an uncertainty of $\pm$ 6.3 for the twenty-four data points used (see Table 5.1). If this ratio, along with the reactor transfer function (global effect) data used in Section III, is substituted into Equation (3.17), a phase angle value of -178.5 degrees is returned for a frequency of 1.0 Hz. Thus, the phase data and the APSD data appear to agree with each other.

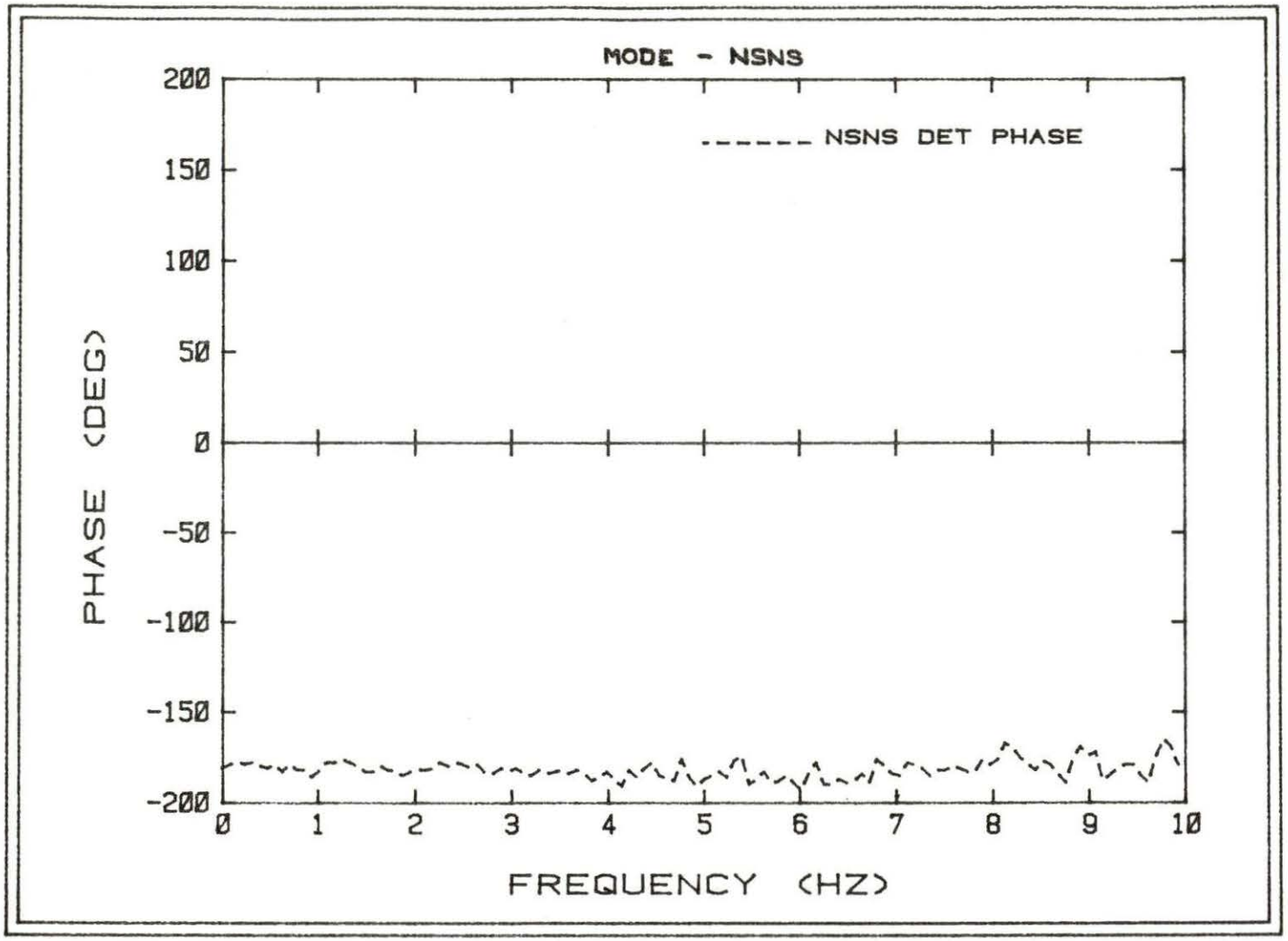

Figure 5.2. Cross-power spectral density phase between the detectors for the NSNS mode

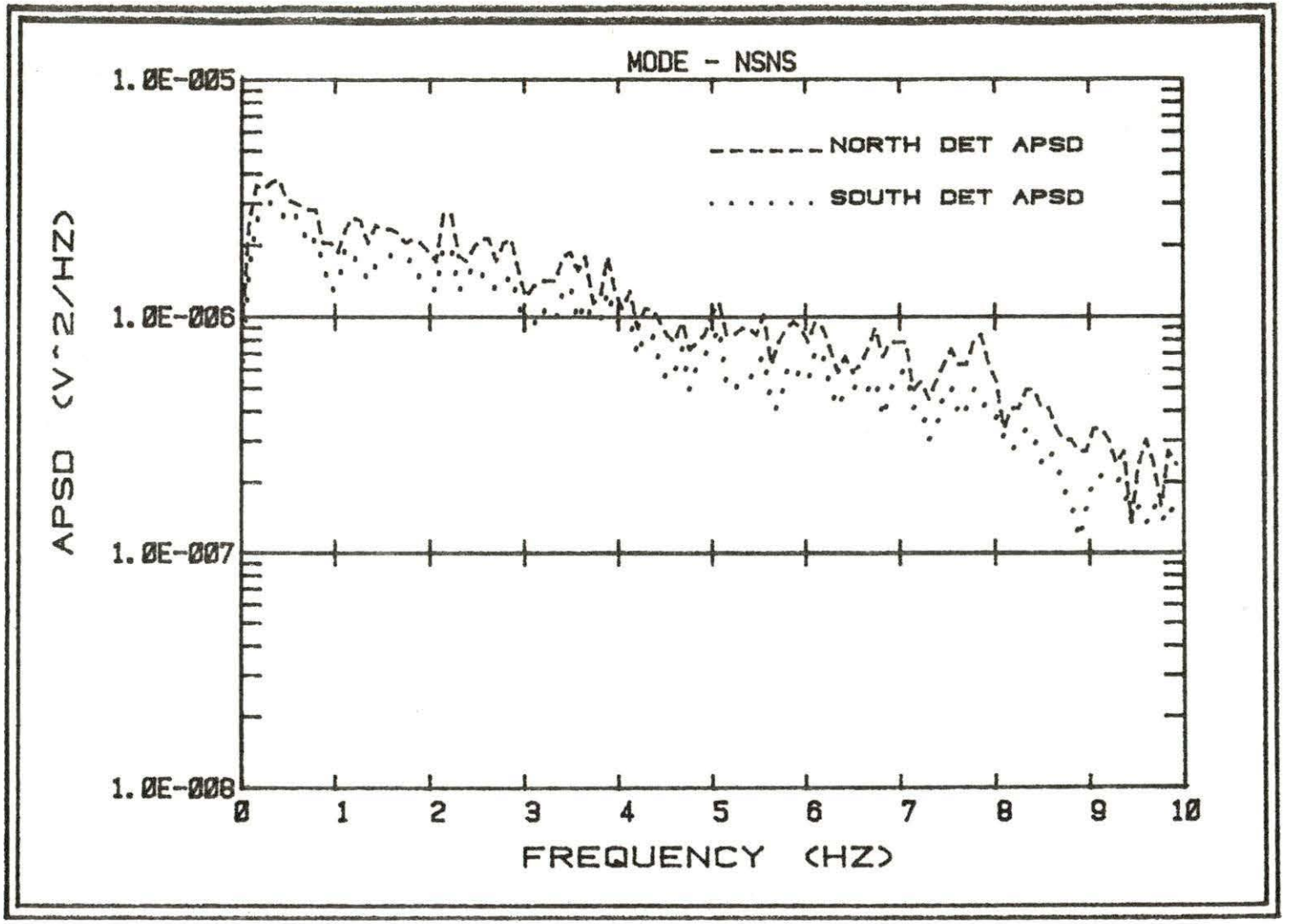

Figure 5.3. Auto-power spectral densities for the detector signals for a PRBS motion input; NSNS mode

Table 5.1. Local-to-global ratios for the various experimental modes

Mode	Input Type	Detector Used	Local-to-Global Ratio	Standard Deviation[a]
NSNS	PRBS	Both	15.8	± 6.3
EWEW	PRBS	Both	23.8	±22.8
NSEW	Sq. Wave (1.0 Hz)	E	0.46	± 0.09
NSEW	Sq. Wave (1.0 Hz)	W	0.30	± 0.07
NSEW	Sq. Wave (3.7 Hz)	E	0.58	± 0.11
NSEW	Sq. Wave (3.7 Hz)	W	0.62	± 0.09
EWNS	Sq. Wave (1.0 Hz)	N	0.59	± 0.11
EWNS	Sq. Wave (1.0 Hz)	S	0.46	± 0.07
EWNS	Sq. Wave (3.7 Hz)	N	0.60	± 0.08
EWNS	Sq. Wave (3.7 Hz)	S	0.73	± 0.12

[a]Standard deviation for NSEW and EWNS modes calculated for 64 ensemble averages using propagation of error method.

The NSNS local-to-global ratio was approximately 4.5 times greater than the one that Al-Ammar calculated in the same manner [1]. This very large difference was probably due to Al-Ammar using a 68 cm by 2.5 cm by 0.64 cm strip of Plexiglas as his vibrator instead of an aluminum rod. Plexiglas behaves similarly to water in a neutron field and has a moderating effect on the neutrons, since it contains a substantial amount of hydrogen [20]. This moderating effect probably affected the thermal flux gradient in a different manner than did the aluminum rod, thus causing a different local-to-global ratio.

From Figure 5.3, it can be seen that the APSD for the south detector was smaller than that of the north detector. This indicated that the local and global effects were cancelling each other to a small degree at the south detector; consequently, the thermal neutron flux gradient must have been sloping downward from north to south, which was consistent with previous measurements and calculations [1,8,9].

In order to test the hypothesis that a vibrating absorber moving in a square wave motion would not generate a harmonic at twice its fundamental frequency, the vibrating absorber was driven by a 1.0 Hertz square wave while the apparatus was in the NSNS mode. Figure 5.4 shows the APSD's for both detectors. It can be seen that the APSD at 2.0 Hertz, which was twice the fundamental frequency,

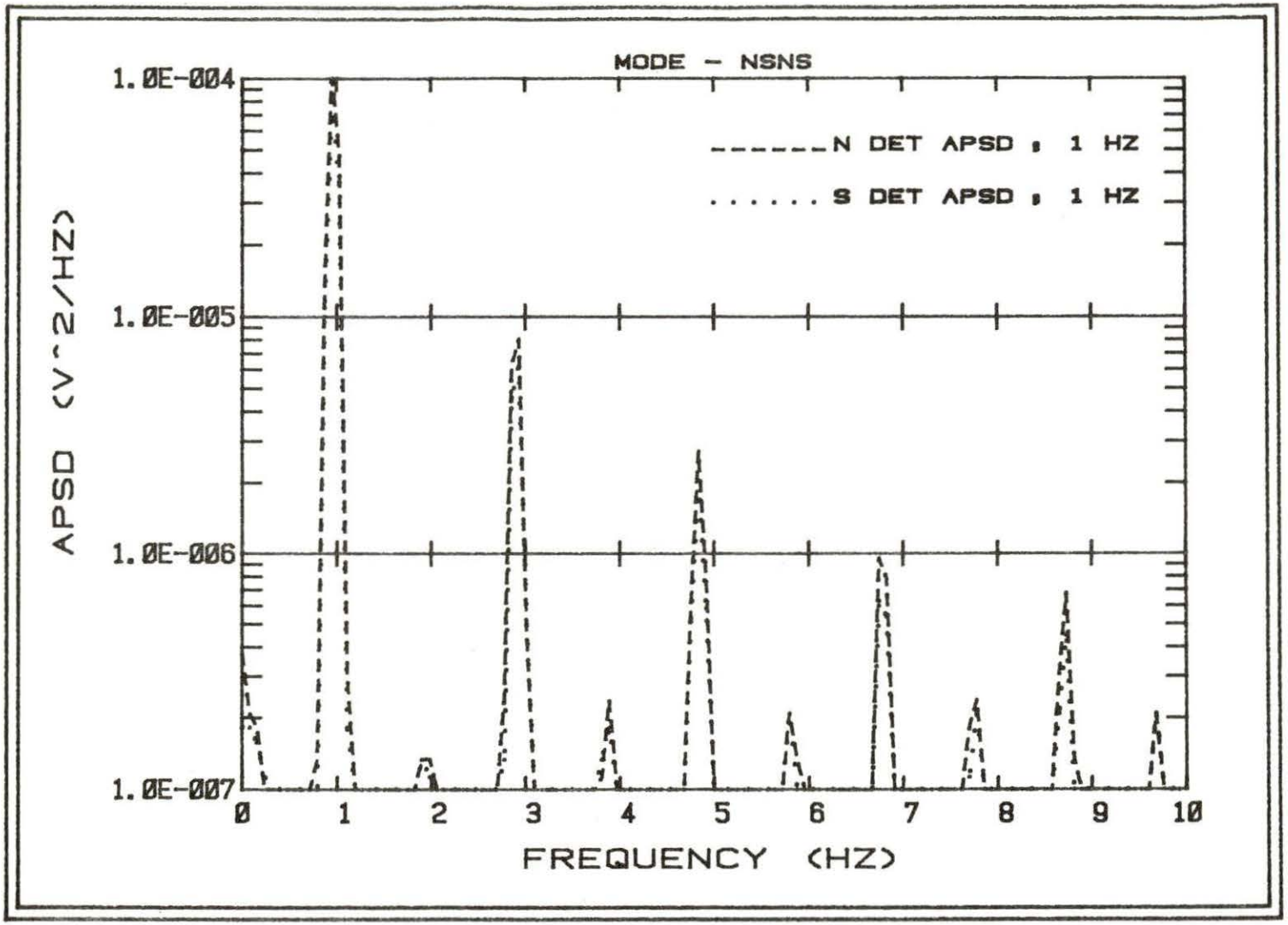

Figure 5.4. Auto-power spectral densities of the detector signals for a square wave motion input of 1.0 Hz; NSNS mode

was about three orders of magnitude less than the peak at the fundamental frequency. Therefore, there was no interference by unwanted harmonics when the apparatus was operated in either the NSEW or EWNS modes.

3. EWEW mode

The local effect also dominated the reactor response when the apparatus was operated in the EWEW mode, as can be seen in Figure 5.5. A comparison of this phase with that shown in Figure 5.2 showed that the EWEW phase was slightly closer to -180^{o} than the NSNS phase. From this comparison, it would be expected that the local-to-global ratio for the EWEW mode would be higher than the ratio for the NSNS mode, which would be consistent with the idea that the flux gradient is flatter in the east-west plane.

Figure 5.6 shows the APSDs of the two detector signals for the EWEW mode. Using these data, LGRAT found a local-to-global ratio of 23.8 with a standard deviation of 22.8. The large standard deviation was caused by two data points with very large local-to-global ratios (around 100). These two points, which occurred at 0.48 Hz and 0.56 Hz, were consistent with the APSD data, since the APSDs for both detectors were almost identical, which was to be expected for a situation where the local-to-global ratio was very large, as it was in this case.

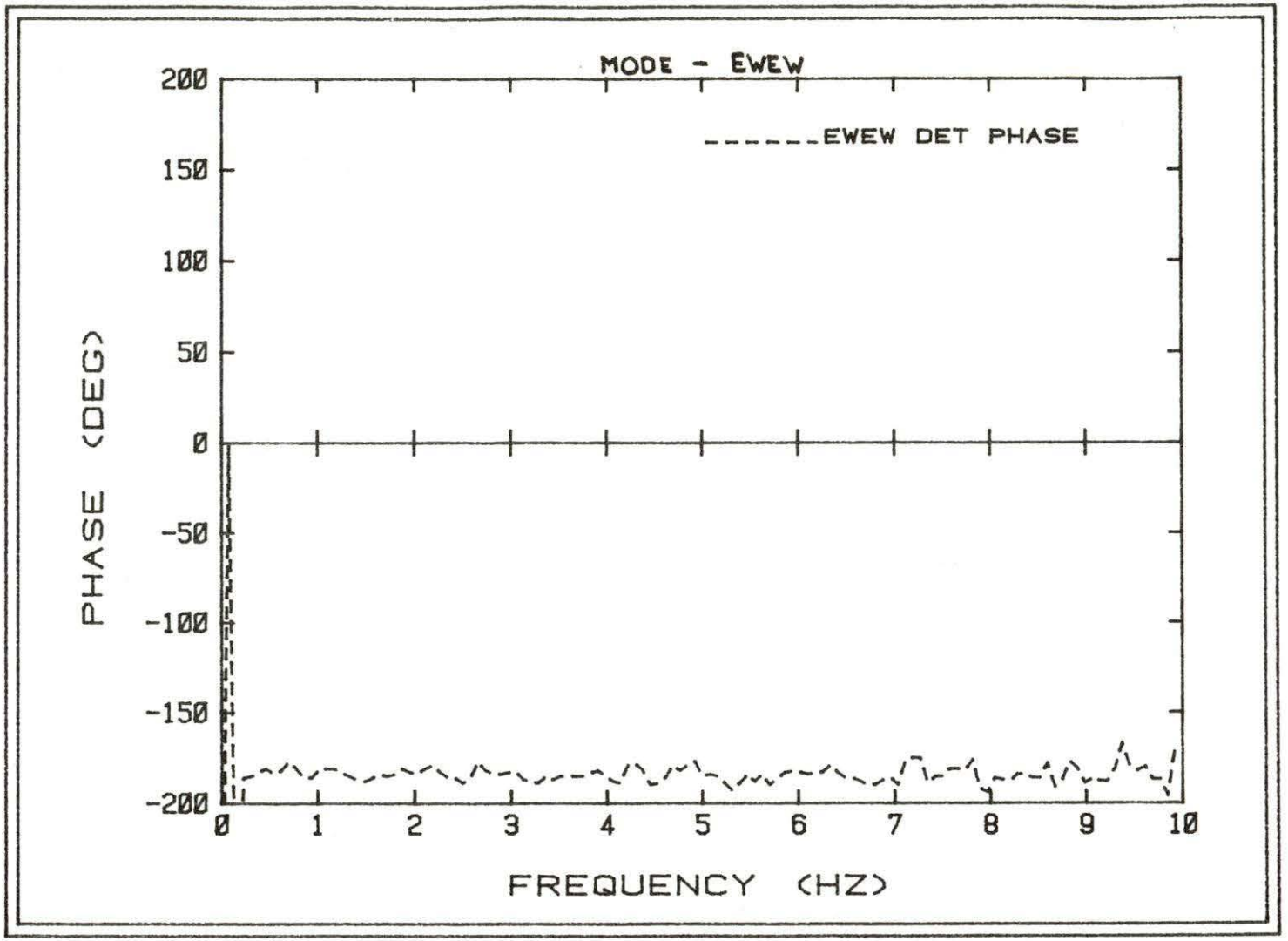

Figure 5.5. Cross-power spectral density phase between the detectors for the EWEW mode

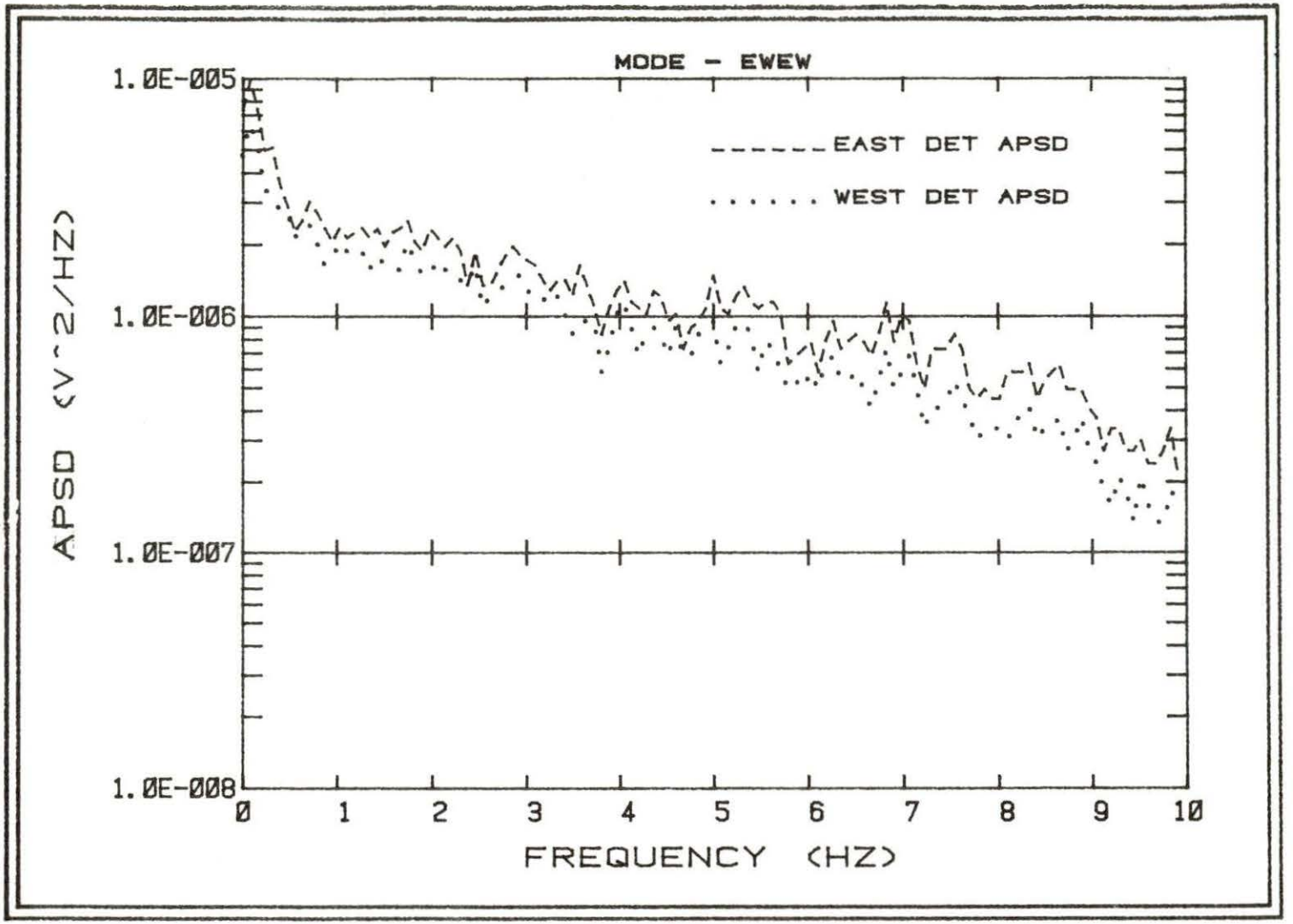

Figure 5.6. Auto-power spectral densities of the detector signals for a PRBS motion input; EWEW mode

The detector phase angle was calculated to be 179 degrees at 1.0 Hz for a local-to-global ratio of 23.8, which was consistent with the phase data.

Al-Ammar concluded that the flux gradient in the east-west plane was nearly flat, since he observed very little global effect from a vibration in that direction [9]. Since the APSDs shown in Figure 5.6 are almost identical and some points generated local-to-global ratios many times greater than the average that was calculated, Al-Ammar's conclusions seem to be verified.

3. NSEW mode

When operated in the NSEW or EWNS modes, the vibrating absorber generated a smaller detector response than when it was in the NSNS or EWEW modes. This was because the detectors did not see as much of a change in the local depression when the absorber was not moving directly toward or away from the detector. Two methods were used to alleviate this problem: (1), the spectrum analyzer sensitivity was increased by a factor of ten, and, (2), the reactor power was increased from 100 watts to 500 watts. The implementation of these two changes increased the magnitude of the detector signals and allowed operation of the spectrum analyzer at a suitable sensitivity.

Figure 5.7 and 5.8 show the APSDs for the two detectors for square wave motion inputs of 1.0 Hertz and 3.7 Hertz, respectively.

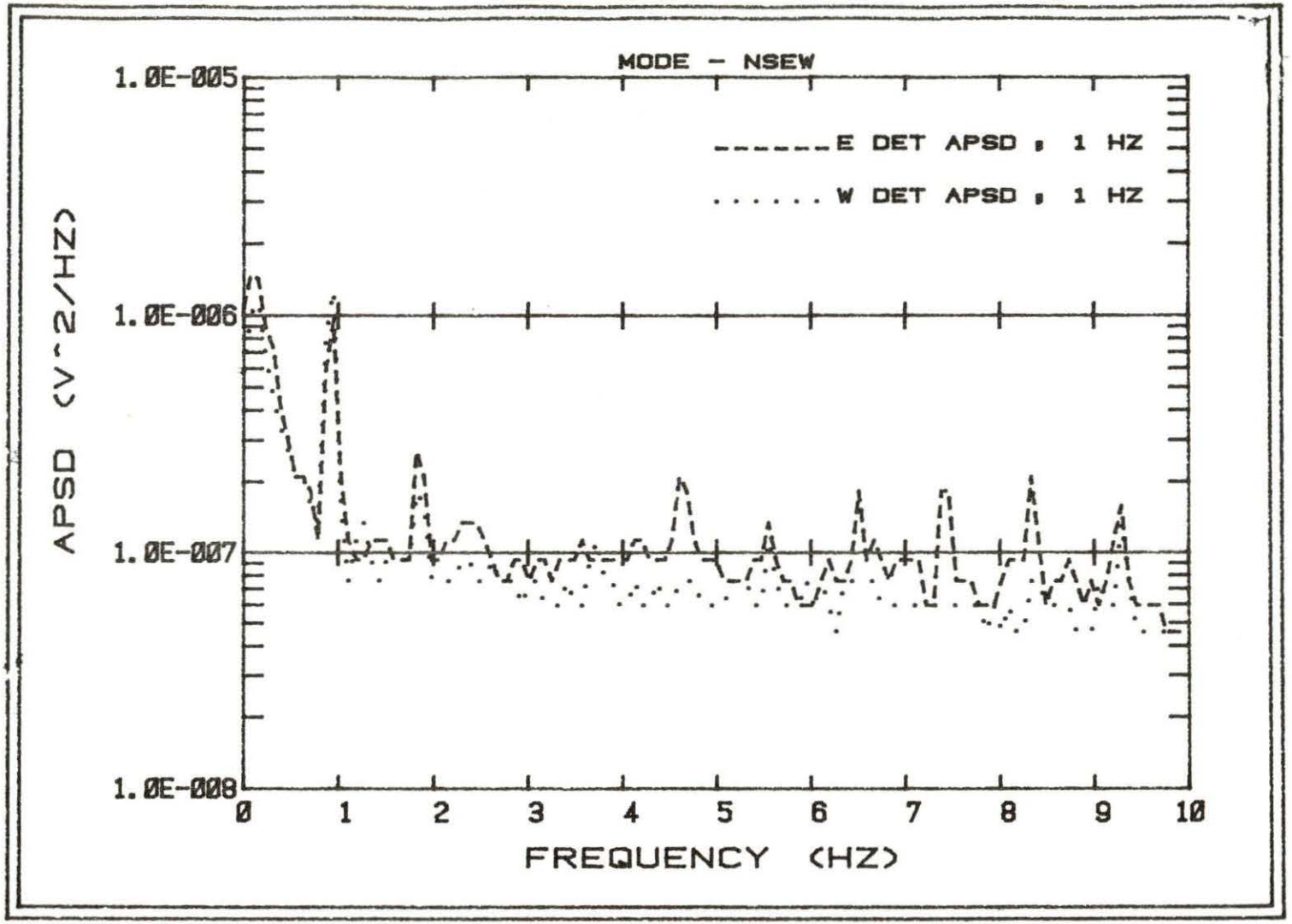

Figure 5.7. Auto-power spectral densities of the detector signals for a square wave motion input of 1.0 Hz; NSEW mode

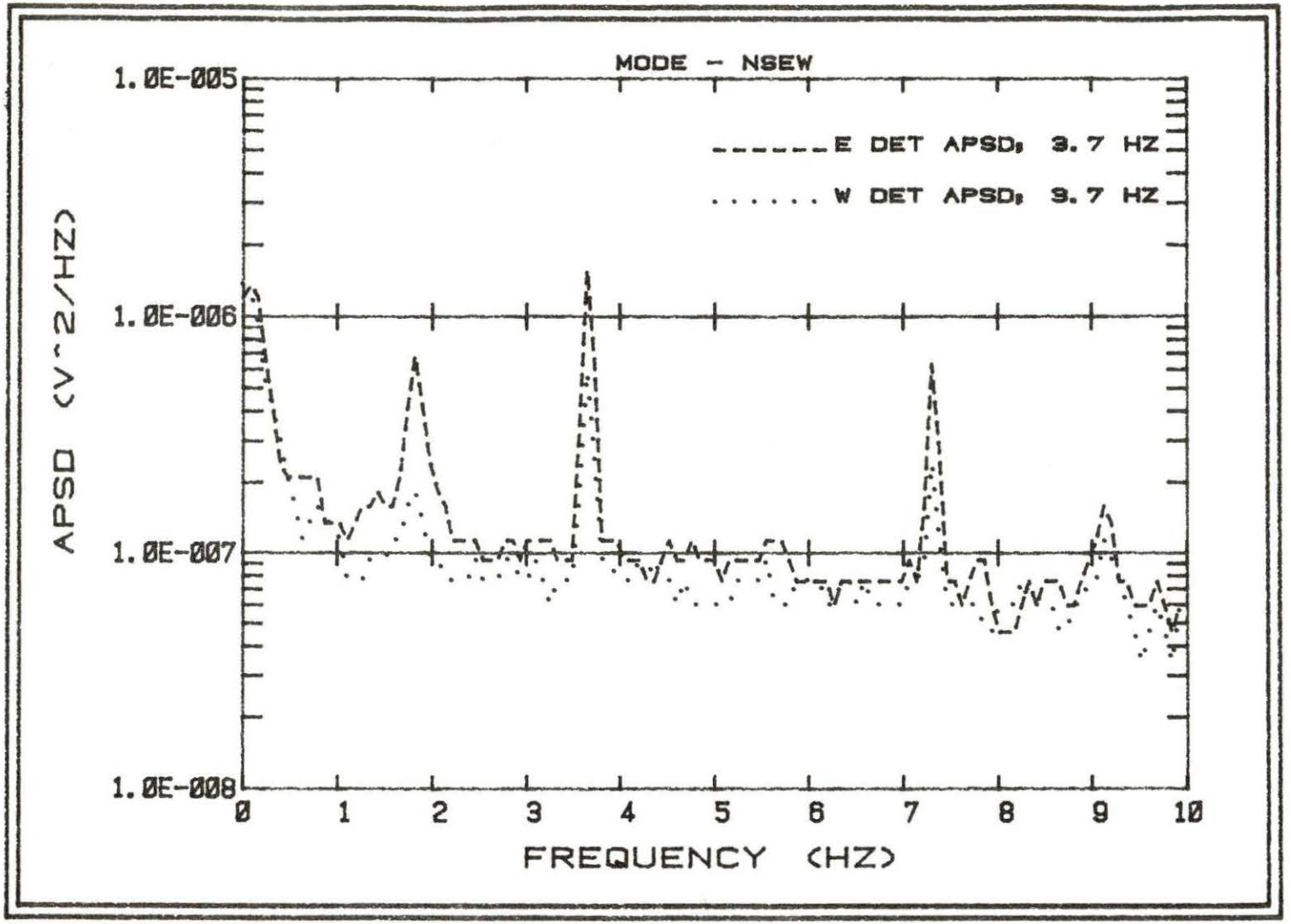

Figure 5.8. Auto-power spectral densities of the detector signals for a square wave motion input of 3.7 Hz; NSEW mode

As might be expected, the APSDs for both detectors were more or less identical, since both detectors saw the same local depression movement and the global effect is space-independent. Using the APSD data shown in these figures and background noise spectrum data, as shown in Figure 5.9, LGRAT calculated, using Equation (3.30), local-to-global ratios for each detector and each input frequency, which are shown in Table 5.1. The differences between the detectors appear to be random, since the east detector gave the higher ratio for the 1.0 Hertz input and the west detector gave the higher ratio for the 3.7 Hertz input. However, for each input frequency, both detectors give, within the margin of uncertainty, about the same local-to-global ratio.

Obviously, the local-to-global ratios seen in this mode are much smaller than those seen in the NSNS or EWEW modes. The reason for this is that the detectors do not see nearly as much of a change in the local flux depression when the absorber is not moving directly towards or away from them. Therefore, the local-to-global ratio is dependent not only upon the distance between the vibrating absorber and the detector, but also upon the direction of the absorber motion with respect to the detector. The local effect will be maximized when the absorber is moving along the line between it and the detector and will be minimized when the absorber is moving perpendicular to that line.

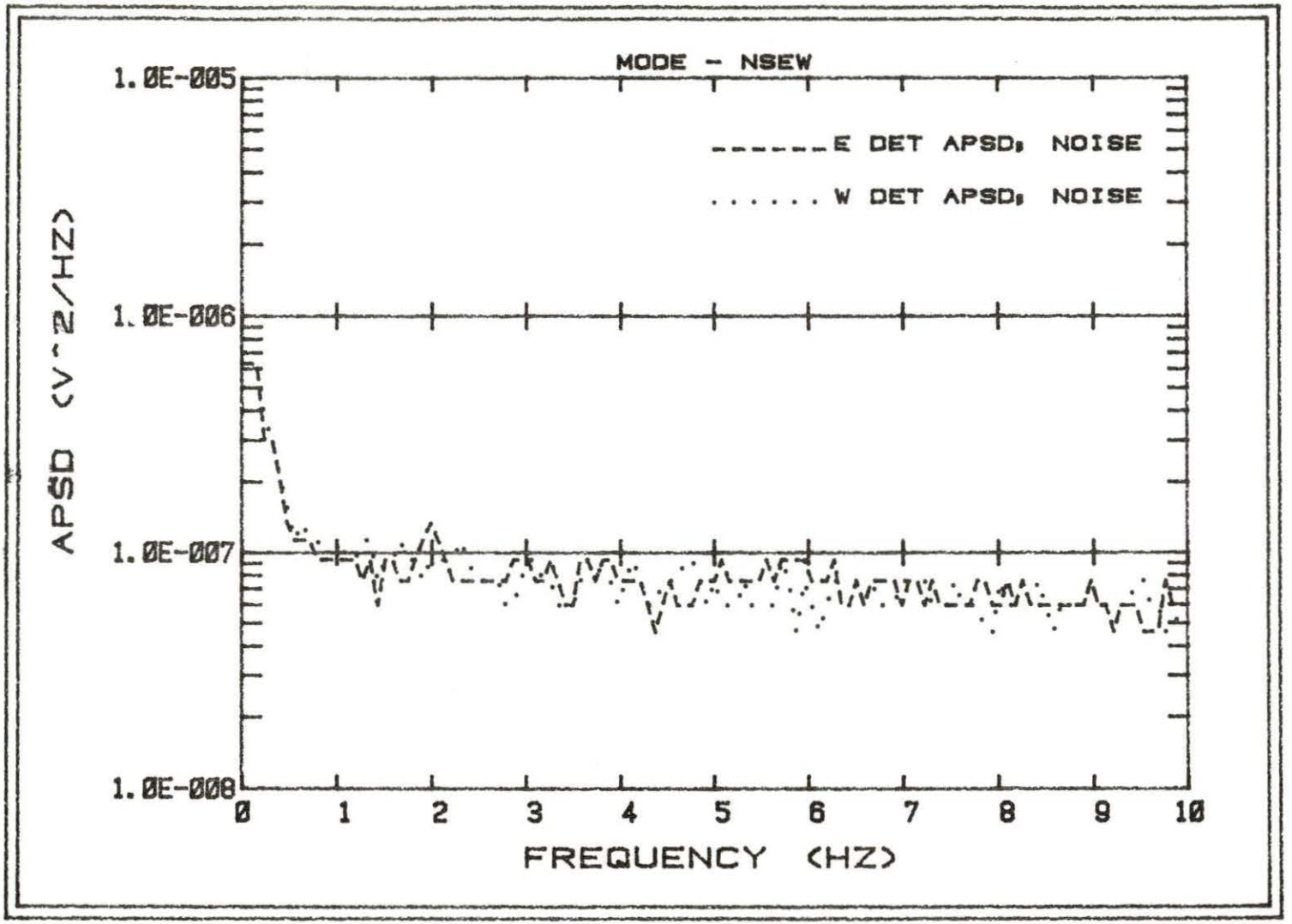

Figure 5.9. Auto-power spectral densities of the reactor background noise for the two detectors; NSEW mode

One interesting feature in Figure 5.8 was the peak at 1.85 Hertz, which was one-half of the input frequency. An examination of the time trace of the LVDT signal showed that every other time that the absorber moved toward the east detector, it did not move as far as it normally did. This caused the input spectrum to be slightly modulated at one-half the square wave frequency. However, this had no effect on the calculations that were made. The peak disappeared after the voltage to the coils was increased slightly, which caused the vibrator to move more firmly and eliminated any variation in the input spectrum.

4. EWNS mode

Figure 5.10 and 5.11 show the APSDs for the two detectors for the 1.0 Hertz and 3.7 Hertz motions, respectively. Again, the APSDs for both detectors are almost identical. The background noise spectrum for these measurements is illustrated in Figure 5.12. With these data, LGRAT calculated local-to-global ratios which are given in Table 5.1. Again, for each input frequency, the local-to-global ratios are about the same, allowing for the uncertainties.

When the average local-to-global ratios were calculated for each frequency, it was clear that the ratios were higher for the EWNS mode than for the NSEW mode. This can again be attributed to the east-west thermal flux gradient being flatter than that along the

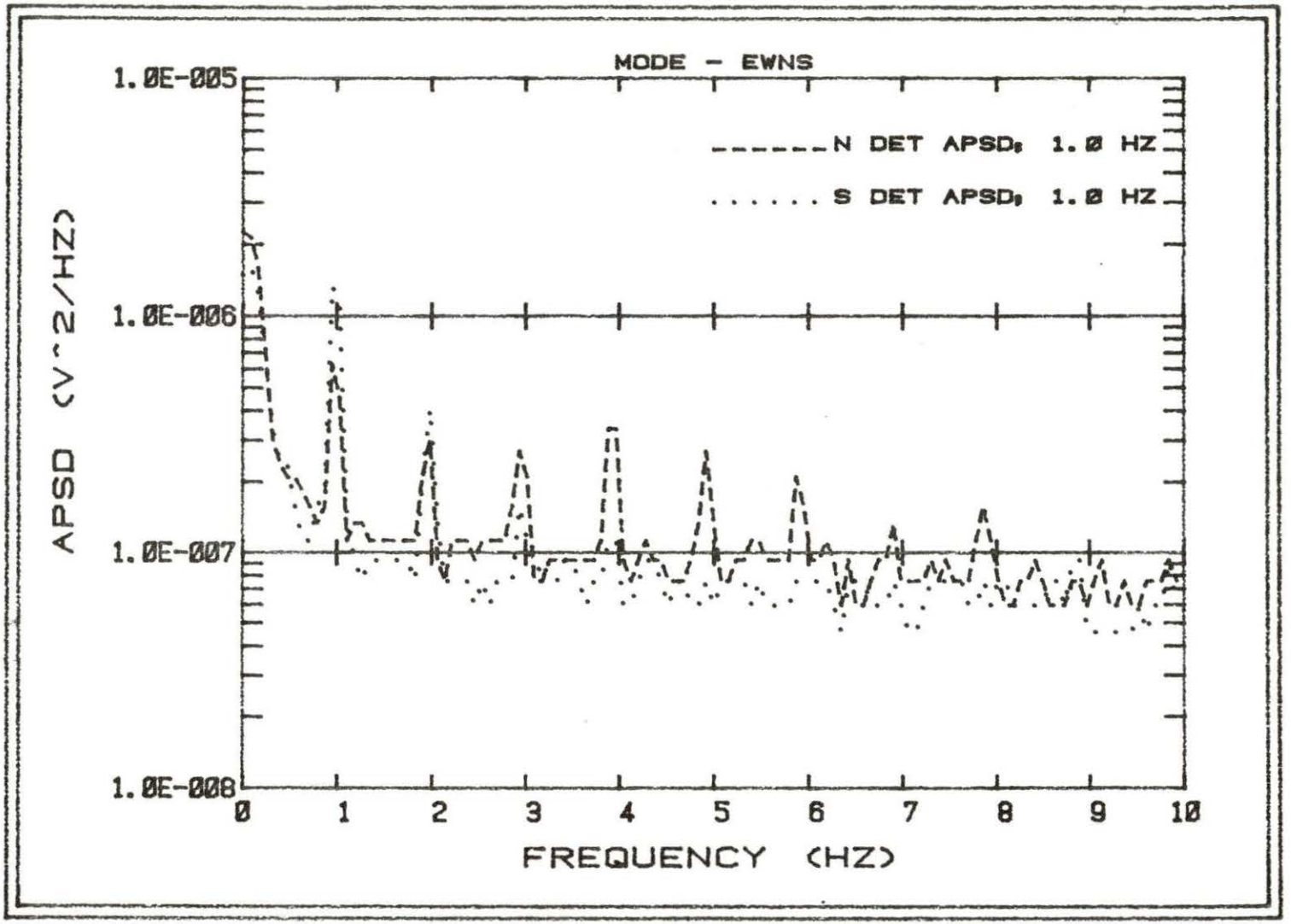

Figure 5.10. Auto-power spectral densities of the detector signals for a square wave motion input of 1.0 Hz; EWNS mode

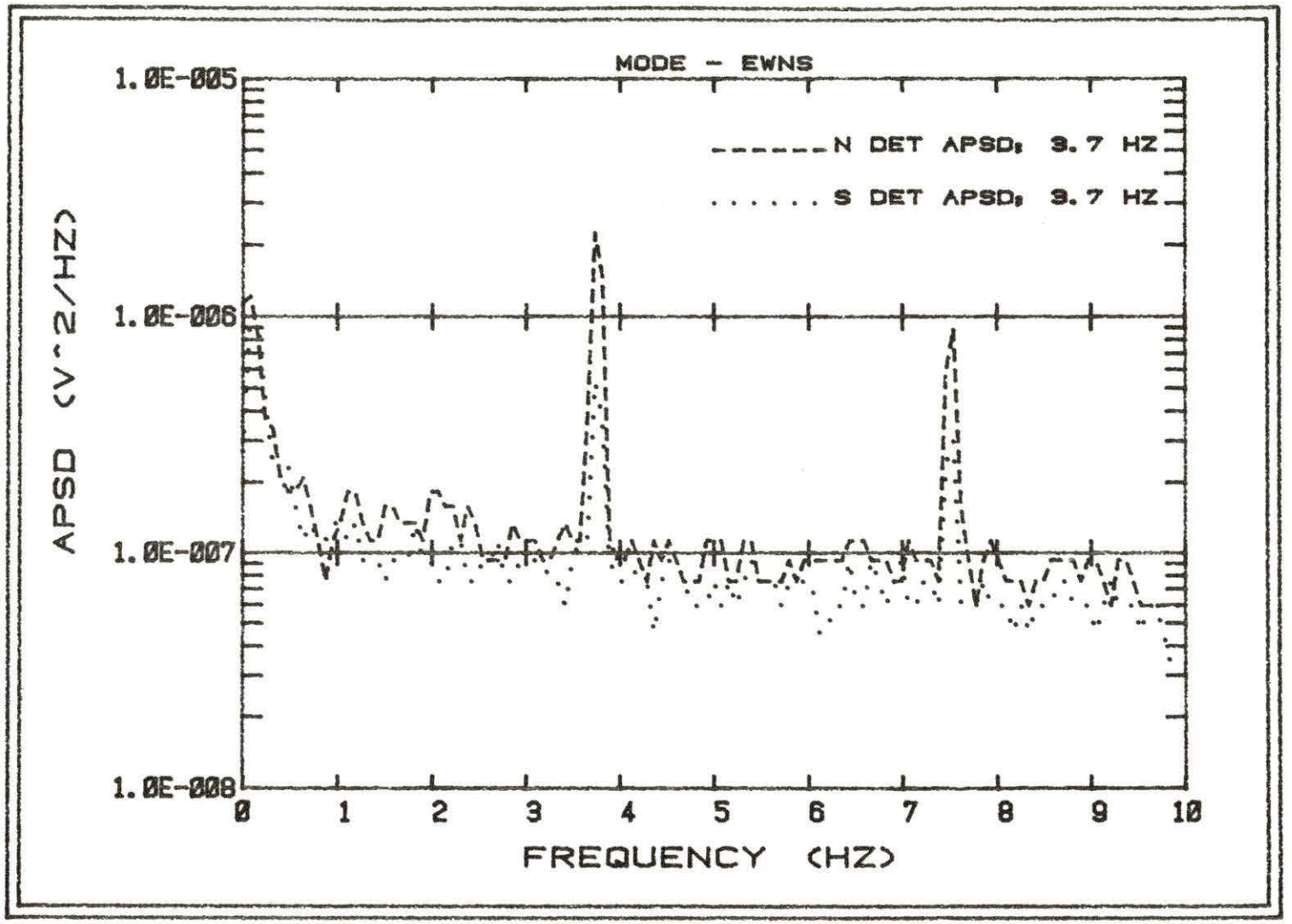

Figure 5.11. Auto-power spectral densities of the detector signals for a square wave motion input of 3.7 Hz; EWNS mode

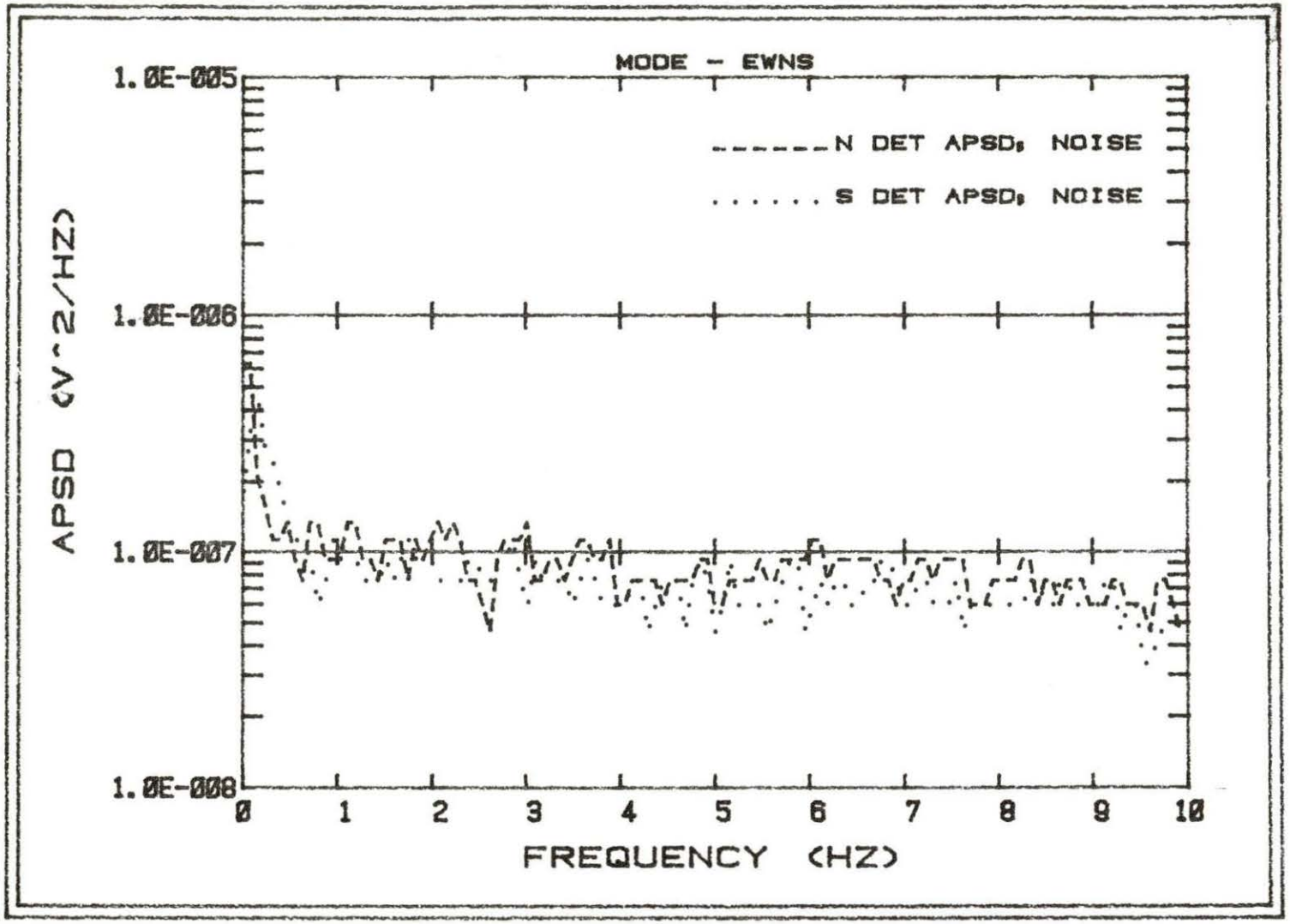

Figure 5.12. Auto-power spectral densities of the reactor background noise for the two detectors; EWNS mode

north-south plane, thus causing a smaller global effect when the absorber moved in the east-west plane. This again supported Al-Ammar's conclusions about the directions and magnitudes of the thermal neutron flux gradients.

VI. CONCLUSIONS

The following are the major conclusions reached through the analysis of the data obtained during this research.

(1) The measurements and calculations that were made verified the results that Al-Ammar found using his apparatus in most ways. The thermal neutron flux gradients determined from the detector responses ran in the same direction as Al-Ammar stated [1]. The major difference between Al-Ammar's results and the results of this research was the much greater magnitude of the local effect seen in this experiment. As was stated earlier, this could have been due to the use of an aluminum vibrator instead of the Plexiglas strip that Al-Ammar used.

(2) The data that were obtained supported the existence of the "double frequency" phenomenon for the local and global effects for the case when the absorber was moving perpendicular to the line between the detectors (NSEW and EWNS modes). The local effect was found to be at twice the frequency of the global effect when the apparatus was operated in these modes.

(3) The magnitude of the local effect is dependent not only upon the distance between the moving absorber and the detector, but also upon the direction of motion of the absorber with

respect to the detector. The local effect will be maximized when the absorber is moving along the line from the absorber to the detector, and will be minimized when the motion is perpendicular to the line between the absorber and the detector.

VII. SUGGESTIONS FOR FUTURE RESEARCH

The following are suggestions that might be considered by future investigators in this field.

(1) A better drive mechanism for the vibrator should be developed. Any drive which uses magnetic coils firing and discharging in close proximity to the detector cables generates electronic noise in those cables, and that noise will be at the same frequency as the neutron noise signals, thus making it difficult to remove by filtering. In this research, several methods were used to block the noise, but a better solution would be to use a noiseless driving device.

(2) The detectors used in future research should be constructed of materials that either do not easily activate or activate to isotopes that have very short half lives, preferably on the order of minutes. Aluminum and Plexiglas are two such materials. This would decrease the amount of "cooling" time required after each run and increase the accessibility of the apparatus for modifications and maintenance.

(3) If possible, the reactor should be operated with the inlet coolant temperature either at or below the ambient temperature of the reactor. This will reduce the humidity inside the reactor, which will in turn reduce condensation and potential

corrosion of some apparatus parts and short circuiting of the apparatus electronics. The negative reactivity associated with the insertion of the apparatus into the CVS should more than make up for the reactivity increase from the cooler, more dense water.

(4) It would be interesting to perturb the thermal neutron flux gradients in the CVS either by inserting poisons into nearby stringers or by reshuffling the fuel loading pattern.

(5) A second interesting experiment would be to construct a cylinderical apparatus that could fit into the CVS in any orientation. A Rotational Variable Displacement Transformer (RVDT) could be employed to measure the exact orientation of the apparatus. The exact direction of the flux gradient could be determined using such an apparatus.

(6) From a theoretical standpoint, it would be interesting to calculate the effect of a vibrating component that not only absorbed neutrons, but also produced neutrons, such as a fuel element. Once a theoretical knowledge was obtained, experimental research could be conducted for this phenomenon using the UTR-10 reactor.

VIII. REFERENCES

1. M. Al-Ammar, Use of local-global ratio in detecting component vibration in reactors, Ph.D. dissertation, Department of Nuclear Engineering, Iowa State University, 1981 (unpublished).

2. H. Van Dam, Neutron noise in boiling water reactors, Atomkernenergie 27, No. 1, 8 (1976).

3. K. Behringer, G. Kosaly, and Lj. Kostic, Theoretical investigation of the local and global components of the neutron-noise field in a boiling water reactor, Nuclear Science and Engineering 63, 306 (1977).

4. I. Pazsit, Investigation of the space-dependent noise induced by a vibrating absorber, Atomkernenergie 30, No. 1, 29 (1977).

5. I. Pazsit, Two group theory of noise in reflected reactors with application to vibrating absorbers, Annals of Nuclear Energy, 5, 185 (1978).

6. I. Pazsit and G. Th. Analytis, Theoretical investigation of the neutron noise diagnostics of two-dimensional control rod vibrations in a PWR, Annals of Nuclear Energy 7, 171 (1980).

7. G. Th. Analytis, A three-dimensional theoretical investigation of the local and global component of neutron noise in bare homogeneous water moderated reactors and applications, Annals of Nuclear Energy 7, 351 (1980).

8. M. Salih, Response of an in-core neutron detector to a vibrating absorber based on the detector adjoint function, M.S. thesis, Department of Nuclear Engineering, Iowa State University, 1971 (unpublished).

9. M. Al-Ammar and R. A. Danofsky, Detection of component vibrations in reactors based on the local-global interaction, Transactions of the American Nuclear Society, Vol. 39, 955 (1981).

10. F. W. Byron and R. W. Fuller, Mathematics of Classical and Quantum Physics (Addison-Wesley, Cambridge, Massachusetts, 1969).

11. J. J. Duderstadt and L. S. Hamilton, Nuclear Reactor Analysis (John Wiley & Sons, New York, 1976).

12. J. S. Bendat and A. G. Piersol, Random Data: Analysis and Measurement Procedures (Wiley-Interscience, New York, 1974).

13. R. G. Brown, Random Signals and Linear Filtering, unpublished manuscript, Department of Electrical Engineering, Iowa State University, copyright 1980.

14. D. L. Hetrick, Dynamics of Nuclear Reactors (The University of Chicago Press, Chicago, 1971).

15. T. C. Chan, Reactor transfer function measurement with the reactor oscillator, M. S. thesis, Department of Nuclear Engineering, Iowa State University, 1971 (unpublished).

16. R. A. Hendrickson, R. A. Danofsky, A. F. Rohach and D. M. Roberts, Safety Analysis Report for the Training Reactor UTR-10, Iowa State University Engineering Research Institute 82418, 1981.

17. LVDT and RVDT Linear and Angular Displacement Transducers, Schaevitz Engineering Technical Bulletin 1002, Pennsauken, New Jersey, 1980.

18. G. F. Knoll, Radiation Detection and Measurement (John Wiley & Sons, New York, 1979).

19. R. A. Hendrickson, private communication, May 1982.

20. D. M. Roberts, private communication, May 1982.

21. M. M. R. Williams, Random Processes in Nuclear Reactors (Pergamon Press, Oxford, 1974).

IX. ACKNOWLEDGEMENTS

The author wishes to express his deepest appreciation to his major professor, Dr. Richard Hendrickson, for the many valuable suggestions and the encouragement that he gave throughout this research. In addition, the author is very grateful to Dr. Richard Danofsky for his discussion and review of many of the theoretical aspects of the research; to Elden Plettner and the operating staff and health physics staff of the UTR-10 reactor, for their hard work and extreme patience; to the staff at the Engineering Research Institute Electronics Shop and Machine Shop; to Mr. Harold Shank of the U.S. Department of Energy Ames Laboratory; to Ms. Jo Sedore and her typewriter; to his fiancee, Ms. Inge Riecke, for her inspiration and patience; and finally, to his parents, Robert and Jean Borland, for their encouragement and support over the past two years.

Funding for this research was provided through a grant from the National Science Foundation (NSF), and the author is greatly indebted to that organization.

X. APPENDIX A: DERIVATION OF THE ONE-DIMENSIONAL RESPONSE

In operator notation, the diffusion equations are [1]

$$\underline{\underline{L}}(\underline{r},t)\underline{\phi}(\underline{r},t)=0, \tag{A.1}$$

where $\underline{\phi}$ is the multigroup neutron flux vector. If a bare, homogeneous, one-dimensional core with two neutron energy groups and one average delayed neutron group is assumed, the diffusion equations are expressed in the form [5]

$$\frac{1}{\nu_1}\frac{\partial\phi_1(x,t)}{\partial t} = D_1(t)\frac{\partial^2\phi_1(x,t)}{\partial x^2} - [\Sigma_{a1}(t) + \Sigma_{R1}(t)]\phi_1(x,t)$$
$$+ (1-\beta)[\nu_1\Sigma_{f1}(t)\phi_1(t) + \nu_2\Sigma_{f2}(t)\phi_2(t)] + \bar{\lambda}C(x,t) \tag{A.2}$$

$$\frac{1}{\nu_2}\frac{\partial\phi_2(x,t)}{\partial t} = D_2(t)\frac{\partial^2\phi_2(x,t)}{\partial x^2} - \Sigma_{a2}(t)\phi_2(x,t)$$
$$+ \Sigma_{R1}(t)\phi_1(x,t), \tag{A.3}$$

and

$$\frac{\partial C(x,t)}{\partial t} = \beta[\nu_1\Sigma_{f1}(t)\phi_1(x,t) + \nu_2\Sigma_{f2}(t)\phi_2(x,t)] - \bar{\lambda}C(x,t), \tag{A.4}$$

where,

ν_1,ν_2 = group averaged neutron speeds

$\phi_1(x,t),\phi_2(x,t)$ = fast and thermal fluxes, respectively,

$\Sigma_{a1}(t),\Sigma_{a2}(t)$ = group averaged macroscopic absorption cross sections,

$\Sigma_{R1}(t)$ = fast group averaged macroscopic removal cross section,

β = average delayed neutron fraction,

ν_1,ν_2 = group averaged prompt neutron release per fission,

$\Sigma_{f1}(t),\Sigma_{f2}(t)$ = group averaged macroscopic fission cross sections,

$\bar{\lambda}$ = average delayed neutron decay constant, and

$C(x,t)$ = delayed neutron precursor concentration.

It is assumed that all fission and delayed neutrons will appear in the fast group.

If only the thermal absorption cross section is perturbed, it is written as a sum of the steady state component and the time-dependent component, or [3],

$$\Sigma_{a2}(t) = \Sigma_{a2o} + \delta\Sigma_{a2}(t). \tag{A.5}$$

This fluctuation will cause perturbations in the fast and thermal fluxes and in the delayed neutron precursor concentration, which are expressed as

$$\phi_i(x,t) = \phi_i(x) + \delta\phi_i(x,t);\ (i=1,2) \tag{A.6}$$

and

$$C(x,t) = C(x) + \delta C(x,t). \tag{A.7}$$

Equations (A.5), (A.6), and (A.7) are substituted into Equations (A.2), (A.3), and (A.4). After expanding all of the terms, the result is simplified by dropping the steady state terms, since they sum to zero. The equations are linearized [21] by neglecting terms that are second order in the fluctuations. This yields

$$\frac{1}{\nu_1}\frac{\partial \delta\phi_1(x,t)}{\partial t} = D_1\frac{\partial^2 \delta\phi_1(x,t)}{\partial x^2} - \Sigma_{a1}\delta\phi_1(x,t) - \Sigma_{R1}\delta\phi_1(x,t)$$

$$+ (1-\beta)\,[\nu_1\Sigma_{f1}\delta\phi_1(x,t) + \nu_2\Sigma_{f2}\delta\phi_2(x,t)] + \bar{\lambda}\delta C(x,t), \qquad (A.8)$$

$$\frac{1}{\nu_2}\frac{\partial \delta\phi_2(x,t)}{\partial t} = D_2\frac{\partial^2 \delta\phi_2(x,t)}{\partial^2 x} - \Sigma_{a2o}\delta\phi_2(x,t) - \delta\Sigma_{a2}(t)\phi_2(x)$$

$$+ \Sigma_{R1}\delta\phi_1(x,t) \qquad (A.9)$$

and

$$\frac{\partial \delta C(x,t)}{\partial t} = \beta[\nu_1\Sigma_{f1}\delta\phi_1(x,t) + \nu_2\Sigma_{f2}\delta\phi_2(x,t)] - \bar{\lambda}\delta C(x,t). \qquad (A.10)$$

After applying the Fourier transform to convert Equations (A.8), (A.9), and (A.10) into the frequency domain, Equation (A.10) may be solved for $C(x,\omega)$, and it is substituted into the transform of Equation (A.16). The resulting frequency domain equations are

$$\frac{j\omega}{\nu_1}\Delta\phi_1(x,\omega) = \frac{D_1\partial^2\Delta\phi_1(x,\omega)}{\partial x^2} - \Sigma_{a1}\Delta\phi_1(x,\omega) - \Sigma_{R1}\Delta\phi_1(x,\omega)$$

$$+ \quad (1-\beta)\left[\nu_1\Sigma_{f1}\Delta\phi_1(x,\omega) + \nu_2\Sigma_{f2}\Delta\phi_2(x,\omega)\right]$$

$$+ \frac{\bar{\lambda}\beta\left[\nu_1\Sigma_{f1}\Delta\phi_1(x,\omega) + \nu_2\Sigma_{f2}\Delta\phi_2(x,\omega)\right]}{\bar{\lambda} + j\omega}, \tag{A.11}$$

and

$$\frac{j\omega}{v_2}\Delta\phi_2(x,\omega) = \frac{D_2\partial^2\Delta\phi_2(x,\omega)}{\partial x^2} - \Sigma_{a2o}\Delta\phi_2(x,\omega) - \Delta\Sigma_{a2}(\omega)\phi_2(x)$$

$$+ \Sigma_{R1}\Delta\phi_1(x,\omega). \tag{A.12}$$

Equations (A.11) and (A.12) are rearranged in terms of the frequency-dependent perturbations. This yields

$$\left[D_1\frac{\partial^2}{\partial x^2} - \frac{j\omega}{v_1} - \Sigma_{a1} - \Sigma_{R1} + (1-\beta)\nu_1\Sigma_{f1} + \frac{\bar{\lambda}\beta\nu_1\Sigma_{f1}}{\bar{\lambda} + j\omega}\right]\Delta\phi_1(x,\omega)$$

$$+ \left[(1-\beta)\nu_2\Sigma_{f2} + \frac{\bar{\lambda}\beta\nu_2\Sigma_{f2}}{\bar{\lambda} + j\omega}\right]\Delta\phi_2(x,\omega) = 0, \tag{A.13}$$

and

$$[\Sigma_{R1}]\Delta\phi_1(x,\omega) + \left[D_2\frac{\partial^2}{\partial x^2} - (\Sigma_{a2o} + \frac{j\omega}{v_2})\right]\Delta\phi_2(x,\omega) = \Delta\Sigma_{a2}(\omega)\phi_2(x). \tag{A.14}$$

Equations (A.13) and (A.14) are rewritten in matrix notation, which yields

$$\begin{bmatrix} D_1 \frac{\partial^2}{\partial x^2} - \frac{j\omega}{\nu_1} + \Sigma_{a1} + \Sigma_{R1} - \nu_1\Sigma_{f1}\left(1 - \frac{j\omega\beta}{\bar{\lambda}+j\omega}\right) & \nu_2\Sigma_{f2}\left(1 - \frac{j\omega\beta}{\bar{\lambda}+j\omega}\right) \\ \Sigma_{R1} & D_2 \frac{\partial^2}{\partial x^2} - \left(\Sigma_{a2o} + \frac{j\omega}{\nu_2}\right) \end{bmatrix}$$

$$\begin{bmatrix} \Delta\phi_1(x,\omega) \\ \\ \Delta\phi_2(x,\omega) \end{bmatrix} = \begin{bmatrix} 0 \\ \\ \Delta\Sigma_{a2}(\omega)\phi_2(x) \end{bmatrix}. \qquad (A.15)$$

Equation (A.15) may be converted back into operator notation, which yields

$$\underline{\underline{L}}(x,\omega)\Delta\underline{\phi}(x,\omega) = \underline{S}(x,\omega), \qquad (A.16)$$

where $\underline{S}(x,\omega)$ is the perturbation source term on the right-hand side of Equation (A.15).

By definition, the adjoint function, $\underline{\psi}^+$, and adjoint operator $\underline{\underline{L}}^+$, are [10]

$$\langle \underline{\underline{L}}\Delta\underline{\phi}, \underline{\psi}^+ \rangle = \langle \Delta\underline{\phi}, \underline{\underline{L}}^+\underline{\psi}^+ \rangle , \qquad (A.17)$$

where [2]

$$\underline{\underline{L}}^+(x,\omega)\underline{\psi}^+(x,\omega) = \underline{\Sigma}_d(x,\omega), \qquad (A.18)$$

where $\underline{\Sigma}_d$ is the frequency-dependent detector cross section.

Equations (A.16) and (A.18) are substituted into Equation (A.17), and if the result is expressed in the integral representation of the inner product, it is written as

$$\int_x \underline{S}(x,\omega)^T \underline{\psi}^+(x,\omega)dx = \int_x \Delta\underline{\phi}(x,\omega)^T \underline{\Sigma}_d(x,\omega)dx. \tag{A.19}$$

The assumption is made that the detector responds only to thermal perturbations. The detector cross section may be described as having a magnitude Q and the detector is located at $x-x_o$ [5]. Therefore,

$$\underline{\Sigma}_d(x,\omega) = \begin{bmatrix} 0 \\ \\ Q\delta(x-x_o) \end{bmatrix}, \tag{A.20}$$

where $\delta(x-x_o)$ is a Dirac delta function located at $x=x_o$. Since, from Equation (A.18), $\underline{\psi}^+$ is a function of $\underline{\Sigma}_d$, then $\underline{\psi}^+$ must also be a function of the detector location, x_o.

If Equation (A.20) is substituted into Equation (A.19) and the right hand integral is evaluated, the result is

$$\Delta\phi_2(x_o,\omega) = \frac{1}{Q}\int_x \Delta\Sigma_{a2}(\omega)\phi_2(x)\psi_2{}^+(x,x_o,\omega)dx. \tag{A.21}$$

Thus, a function has been calculated which describes the perturbation that a thermal neutron detector at $x=x_o$ would see if a fluctuation in the thermal absorption cross section was occuring somewhere in the reactor.

In the case of a vibrating absorber inducing a perturbation, the absorber may be modeled as a thermal neutron absorbing plate of strength located at $x=x_p$. Thus [5],

$$\sum_{a2}^{\text{plate}} = \gamma\delta(x-x_p). \tag{A.22}$$

Since the plate is vibrating, x_p must vary temporally and can, therefore, be described as having a steady state or equilibrium location, x_p, plus a time varying component of relatively small amplitude, $\varepsilon(t)$. Therefore,

$$x_p(t) = x_p + \varepsilon(t). \tag{A.23}$$

The mathematical form of the perturbation is, in the time domain [5],

$$\delta\Sigma_{a2} = \gamma \left\{\delta[x-x_p-\varepsilon(t)] - \delta(x-x_p)\right\}. \tag{A.24}$$

Equation (A.24) is inserted into Equation (A.21), which yields

$$\Delta\phi_2(x_o,\omega) = \frac{\gamma}{Q}\int_{-\infty}^{+\infty}\int_{X} \left\{\delta[x-x_p-\varepsilon(t)] - \delta(x-x_p)\right\} \phi_2(x)\psi_2^{+}(x,x_o,\omega)dx$$

$$\exp(-j\omega t)dt. \tag{A.25}$$

If Equation (A.25) is integrated over the reactor, the result is

$$\Delta\phi_2(x_o,\omega) = \frac{\gamma}{Q}\int_{-\infty}^{+\infty}\Big\{\phi_2[x_p+\varepsilon(t)]\psi_2^{+}[x_p+\varepsilon(t),x_o,\omega]$$

$$-\phi_2(x_p)\psi_2^{+}(x_p,x_o,\omega)\Big\}\exp(-j\omega t)dt. \qquad (A.26)$$

Equation (A.26) may be expanded in a Taylor series of $\varepsilon(t)$. Since the vibrator has been assumed to have a small motion amplitude, terms greater than first order in $\varepsilon(t)$ may be neglected. If the Fourier transform is then applied to bring all terms into the frequency domain, the result is

$$\Delta\phi_2(x_o,\omega) = \frac{\gamma}{Q}\left[\phi_2(x_p)\left.\frac{\partial\psi_2^{+}(x,x_o,\omega)}{\partial x}\right|_{x=x_{p-}+0}\right.$$

$$+\left.\psi_2^{+}(x_p,x_o,\omega)\left.\frac{\partial\phi_2(x)}{\partial x}\right|_{x=x_p}\right]\varepsilon(\omega). \qquad (A.27)$$

It may be noted that the adjoint gradient cannot be evaluated exactly at $x=x_p$, since the adjoint gradient does not exist at this point [5]. Consequently, the adjoint gradient must be evaluated at some point very near x_p, i.e., $x=x_{p-}+0$.

XI. APPENDIX B: REDUCTION OF ELECTRONIC NOISE PICKUP IN THE DETECTOR SIGNAL CHANNELS

One of the major problems encountered in this research was that of unwanted electronic noise being generated in the detector signal channels. This noise had a tendency to mask the useful noise signals, making it difficult to analyze the useful noise. Consequently, the elimination of this unwanted noise was an important step in conducting the experiment.

There were, generally speaking, two types of unwanted noise that were present in the signal channels: (1) noise outside the frequency range of interest of 1 to 10 Hertz, and, (2) noise that falls in that frequency range. The former type was mainly 60 Hertz noise from other electronic equipment, small DC offsets from the equipment, and the DC component of the detector signals. Although these noise sources were outside the frequency range of interest, their amplitudes were great enough to overload the spectrum analyzer unless it was operated at a very low sensitivity making useful measurements of the reactor noise impossible.

In order to protect the signal cables from 60 Hertz noise pickup, all of the cables including those in the detector-battery-preamp loops, were shielded with a copper braid. The braids were connected to the cases of all of the instruments, such as the preamps and filters. These cases were isolated from the

actual circuitry inside them. In order to be sure that no ground loops existed, all instrument cases and cable braids were connected to a single ground braid which was connected to the main ground bus in the UTR-10 reactor control panel.

Since the outer shells of the detectors were actually part of the circuit, it was necessary to shield them from potential 60 Hertz noise pickup as well. In order to do this, the detectors were first covered with a layer of insulating plastic. Around the plastic was wrapped a layer of aluminum foil, which acted as the shielding material. The aluminum foil was connected to the braids on the detector cables, which eventually led back to the ground bus. The aluminum foil was covered with another layer of plastic for insulation.

Any 60 Hertz noise pickup that was able to penetrate the shielding and get into the signal cables was almost completely blocked from the spectrum analyzer inputs by the fourth-order low pass filters. With their cutoff frequency set at 12.0 Hertz, each filter attenuated 60 Hertz noise pickup by -56 db with respect to the frequency range of interest.

The unwanted DC component of the noise was eliminated in two ways. First, the second-order high pass filter, with its 0.097 Hertz cutoff, strongly attenuated the DC component of the detector

signal. Second, the DC offset adjustment potentiometers in the fourth-order low pass filters were used to balance any DC offsets that were present in the instrumentation.

The noise that fell within the frequency range of interest was caused mainly by the oscillating magnetic fields generated by the coils. The noise generated by the magnetic fields was about the same magnitude as the useful signals from the detectors. These fields were very strong, and it was difficult to reduce the noise produced by them.

The first measure used was to surround the magnetic coils with layers of magnetic shielding metal, which helped to attenuate the magnetic fields. While this reduced much of the noise, there was still a significant amount present in the detector signals. It was found that grounding the aluminum box housing the coils also reduced the noise. The cables between the detectors and the batteries and preamps had to pass through the coil-housing box, and it was demonstrated that the copper braids surrounding the cables were too permeable to significantly attentuate the magnetic fields. Therefore, the length of each cable that passed through the box was covered with aluminum foil connected to the ground bus. This measure, combined with the other two, reduced the level of noise generated by the oscillating magnetic fields from the coils by at least two orders of magnitude to a signal-to-noise ratio of 100:1.

XII. APPENDIX C: LISTING OF COMPUTER PROGRAMS

A. DATSTR (DATa STоRage)

```
10 OPTION BASE 1
20 DIM A$[2560],B(130)
30 J=1
40 REMOTE 711
50 OUTPUT 711 ;"LDS"
60 ENTER 711 ; A$
70 OUTPUT 711 ;"LSP"
80 ENTER 711 ; F
90 LOCAL 711
100 CLEAR
110 BEEP
120 DISP "INPUT NAME OF DATA STORAGE FILE"
130 INPUT N$
140 CREATE N$,1,1280
150 ASSIGN# 1 TO N$
160 FOR I=1 TO 1280 STEP 10
170 B(J)=VAL(A$[I])
180 PRINT# 1 ; B(J)
190 J=J+1
200 NEXT I
210 F=F/125*127
220 PRINT# 1 ; F
230 ASSIGN# 1 TO *
240 BEEP
250 DISP "END"
260 END
```

B. APSD (APSD calculator)

```
10 DIM G(150),G1(150)
20 CLEAR
30 BEEP
40 DISP "INPUT NAME OF RAW DATA STORAGE FILE"
50 INPUT M$
60 ASSIGN# 1 TO M$
70 BEEP
80 DISP "INPUT NAME OF APSD DATA STORAGE FILE"
90 INPUT N$
100 CREATE N$,1,1280
110 ASSIGN# 2 TO N$
120 FOR I=1 TO 128
130 READ# 1 ; G(I)
140 G1(I)=G(I)^2
150 PRINT# 2 ; G1(I)
160 NEXT I
170 READ# 1 ; F
180 PRINT# 2 ; F
190 ASSIGN# 1 TO *
200 ASSIGN# 2 TO *
210 CLEAR
220 BEEP
230 DISP "DO YOU WANT A HARD COPY OF THE APSD DATA? (Y OR N)
"
240 INPUT A$
250 IF A$<>"Y" THEN 340
260 IMAGE " FREQ (HZ)",10X,"APSD"
270 PRINT USING 260
280 FOR I=1 TO 128
290 F1=F/127*(I-1)
300 PRINT USING 310 ; F1,G1(I)
310 IMAGE D.DDDE,8X,D.DDDE
320 NEXT I
330 BEEP
340 DISP "END"
350 END
```

C. CPSD (CPSD magnitude calculator)

```
10 DIM G1(150),G2(150),H(150)
20 CLEAR
30 BEEP
40 DISP "INPUT NAME OF APSD DATA STORAGE FILE FOR INPUT CHAN
NEL"
50 INPUT A$
60 ASSIGN# 1 TO A$
70 DISP "INPUT NAME OF TRANSFER FUNCTION MAGNITUDE DATA STOR
AGE FILE"
80 INPUT B$
90 ASSIGN# 2 TO B$
100 DISP "INPUT NAME OF CPSD MAGNITUDE DATA STORAGE FILE"
110 INPUT C$
120 CREATE C$,1,1280
130 ASSIGN# 3 TO C$
140 FOR I=1 TO 128
150 READ# 1 ; G1(I)
160 READ# 2 ; H(I)
170 G2(I)=G1(I)*H(I)
180 PRINT# 3 ; G2(I)
190 NEXT I
200 READ# 1 ; F
210 PRINT# 3 ; F
220 ASSIGN# 1 TO *
230 ASSIGN# 2 TO *
240 ASSIGN# 3 TO *
250 CLEAR
260 BEEP
270 DISP "DO YOU WANT A HARD COPY OF THE CPSD MAGNITUDE DATA
? (Y OR N)"
280 INPUT D$
290 IF D$<>"Y" THEN 370
300 IMAGE " FREQ (HZ)",10X,"CPSD MAG"
310 PRINT USING 300
320 FOR I=1 TO 128
330 F1=F/127*(I-1)
340 PRINT USING 350 ; F1,G2(I)
350 IMAGE D.DDDE,8X,D.DDDE
360 NEXT I
370 BEEP
380 DISP "END"
390 END
```

D. LGRAT (Local-to-Global RATio calculator)

```
10 DIM J(30),K(30),R(30)
20 PRINTER IS 710,132
30 CLEAR
40 BEEP
50 DISP " DETECTORS IN LINE (TYPE 1) OR OUT OF LINE WITH VIB
RATION (TYPE 2) ?"
60 INPUT X
70 IF X=2 THEN 550
80 BEEP
90 DISP " INPUT NAMES OF ASPD DATA STORAGE FILES (NORTH OR E
AST FIRST) "
100 INPUT A$,B$
110 ASSIGN# 1 TO A$
120 ASSIGN# 2 TO B$
130 FOR I=1 TO 2
140 READ# 1 ; D
150 READ# 2 ; D
160 NEXT I
170 BEEP
180 DISP " IS THE DETECTOR PHASE BETWEEN 0 AND -90 (TYPE 1)
OR BETWEEN -90 AND -180 (TYPE 2) ? "
190 INPUT Y
200 N=0
210 Q=0
220 Q1=0
230 FOR I=3 TO 26
240 READ# 1 ; J(I)
250 READ# 2 ; K(I)
260 F=.08*(I-1)
270 IF J(I)<=K(I) THEN 370
280 S=SQR(J(I))
290 T=SQR(K(I))
300 U=S+T*(-1)^Y
310 V=S-T*(-1)^Y
320 R(I)=U/V
330 PRINT USING 400 ; F,R(I)
340 Q=Q+R(I)
350 Q1=Q1+R(I)^2
360 GOTO 390
370 PRINT USING 420 ; F
380 N=N+1
390 NEXT I
400 IMAGE ZZ.DD,7X,ZZZZ.DD
410 A=Q/(24-N)
420 IMAGE ZZ.DD,7X,"INF"
430 PRINT USING 440 ; A
440 IMAGE " AVERAGE LOCAL-GLOBAL RATIO=",ZZZ.DD
```

```
450 S1=SQR(Q1/(24-N)-A^2)
460 IMAGE " STANDARD DEVIATION=",ZZZ.DD
470 PRINT USING 460 ; S1
480 ASSIGN# 1 TO *
490 ASSIGN# 2 TO *
500 P=N/24*100
510 PRINT USING 520 ; P
520 IMAGE " PERCENT OF DATA UNUSED=",ZZZ.D
530 PRINTER IS 2
540 GOTO 1080
550 CLEAR
560 BEEP
570 DISP " INPUT NAME OF APSD FILE AND NAME OF BACKGROUND FI
LE"
580 INPUT A$,N$
590 ASSIGN# 1 TO A$
600 ASSIGN# 2 TO N$
610 CLEAR
620 BEEP
630 DISP " INPUT LOWER AND UPPER FREQUENCY BOUNDS FOR GLOBAL
 (FUNDAMENTAL) PEAK"
640 INPUT F1,F2
650 DISP " INPUT LOWER AND UPPER BOUNDS FOR LOCAL PEAK"
660 INPUT F3,F4
670 F5=F1/.08+1
680 F6=F2/.08+1
690 F7=F3/.08+1
700 F8=F4/.08+1
710 FOR I=1 TO F5-1
720 READ# 1 ; D
730 READ# 2 ; D
740 NEXT I
750 I1=0
760 I2=0
770 FOR I=F5 TO F6
780 READ# 1 ; V1
790 READ# 2 ; V2
800 I1=V1-V2+I1
810 NEXT I
820 FOR I=F6+1 TO F7-1
830 READ# 1 ; D
840 READ# 2 ; D
850 NEXT I
860 PRINTER IS 710,132
870 FOR I=F7 TO F8
880 READ# 1 ; V1
890 READ# 2 ; V2
900 I2=V1-V2+I2
910 NEXT I
920 R=SQR(I2/I1)
```

```
930 IMAGE " GLOBAL PEAK FREQUENCY RANGE - ",D.DD," HZ TO ",D
.DD," HZ"
940 IMAGE " CORRECTED GLOBAL INTEGRAL = ",D.DDE
950 IMAGE " LOCAL PEAK FREQUENCY RANGE - ",D.DD," HZ TO ",D.
DD," HZ"
960 IMAGE " CORRECTED LOCAL INTEGRAL = ",D.DDE
970 IMAGE " LOCAL-TO-GLOBAL RATIO = ",DDD.DDD
980 ASSIGN# 1 TO *
990 ASSIGN# 2 TO *
1000 PRINT USING 930 ; F1,F2
1010 PRINT USING 940 ; I1
1020 PRINT
1030 PRINT USING 950 ; F3,F4
1040 PRINT USING 960 ; I2
1050 PRINT
1060 PRINT USING 970 ; R
1070 PRINTER IS 2
1080 BEEP
1090 DISP "END"
1100 END
```

E. PLOT5 (magnitude PLOTter no. 5)

```
10 OPTION BASE 1
20 DIM B(270),C$[50]
30 CLEAR
40 BEEP
50 DISP " INPUT NAME OF DATA FILE FROM WHICH DATA IS TO BE P
LOTTED"
60 INPUT A$
70 ASSIGN# 1 TO A$
80 CLEAR
90 BEEP
100 DISP "INPUT DESIRED LINETYPE BY NUMBER"
110 INPUT K
120 N=128
130 X=0
140 FOR I=1 TO N
150 READ# 1 ; B(I)
160 IF B(I)<X THEN 180
170 X=B(I)
180 NEXT I
190 DISP " SELECT HIGHEST VERTICAL VALUE (TYPE 1) OR AUTOMAT
IC SELECTION (TYPE 2)? "
200 INPUT Q
210 IF Q=2 THEN 250
220 DISP " INPUT HIGHEST VALUE"
230 INPUT H
240 GOTO 270
250 X=INT(LGT(X))
260 H=10^(X+1)
270 READ# 1 ; F
280 IF K<>1 THEN F=F*125/127
290 IF K<>1 THEN N=126
300 ASSIGN# 1 TO *
310 PLOTTER IS 705
320 LOCATE 35,115,30,90
330 SCALE 0,F,LOG(H/1000),LOG(H)
340 CLEAR
350 BEEP
360 DISP " DO YOU NEED AXES AND AXIS LABELS? (Y OR N)"
370 INPUT D$
380 IF D$<>"Y" THEN 780
390 CLEAR
400 BEEP
410 DISP " INPUT VERTICAL AXIS LABEL"
420 INPUT L$
```

```
430 FOR I=4 TO 1 STEP -1
440 XAXIS LOG(H/10^(I-1)),F/10
450 NEXT I
460 YAXIS 0
470 YAXIS F
480 FOR I=4 TO 1 STEP -1
490 FOR J=2 TO 9
500 MOVE 0,LOG(J*H/10^(I-1))
510 DRAW .02*F,LOG(J*H/10^(I-1))
520 NEXT J
530 NEXT I
540 FOR I=4 TO 1 STEP -1
550 FOR J=2 TO 9
560 MOVE F,LOG(J*H/10^(I-1))
570 DRAW .98*F,LOG(J*H/10^(I-1))
580 NEXT J
590 NEXT I
600 IMAGE D.DE
610 FOR I=4 TO 1 STEP -1
620 MOVE -.01*F,LOG(H/10^(I-1)) @ LORG 8
630 LABEL USING 600 ; H/10^(I-1)
640 NEXT I
650 MOVE 0,LOG(.87*H/1000) @ LORG 6
660 IMAGE D
670 LABEL USING 660 ; 0
680 FOR I=2 TO 11
690 MOVE (I-1)*F/10,LOG(.87*H/1000) @ LORG 6
700 LABEL USING "2D" ; (I-1)*F/10
710 NEXT I
720 MOVE 3*F/10,LOG(.47*H/1000)
730 LORG 1 @ CSIZE 3,1,0
740 LABEL "FREQUENCY (HZ)"
750 MOVE -F/5,LOG(H/100) @ LORG 3
760 DEG @ LDIR 90
770 LABEL L$
780 LINETYPE K,1
790 IF B(1)<H/1000 THEN B(1)=H/1000
800 MOVE 0,LOG(B(1))
810 FOR I=2 TO N
820 IF B(I)<H/1000 THEN B(I)=H/1000
830 PLOT (I-1)*F/N,LOG(B(I)),-1
840 NEXT I
850 PENUP
860 CLEAR
870 BEEP
880 LDIR 0
890 DISP " WOULD YOU LIKE A LEGEND FOR THE PLOT? (Y OR N) "
900 INPUT Q$
910 IF Q$<>"Y" THEN 1100
920 DISP "POSITION 1 OR 2?"
930 INPUT T
```

```
940 LORG 1 @ CSIZE 2,1,0
950 DISP " INPUT LEGEND LABEL"
960 INPUT T$
970 IF T=2 THEN 1040
980 MOVE F/2,LOG(.5*H)
990 LINETYPE K,1
1000 DRAW .62*F,LOG(.5*H)
1010 MOVE .63*F,LOG(.5*H)
1020 LABEL T$
1030 GOTO 1100
1040 MOVE .5*F,LOG(.3*H)
1050 LINETYPE K,1
1060 DRAW .62*F,LOG(.3*H)
1070 MOVE .63*F,LOG(.3*H)
1080 LABEL T$
1090 PENUP
1100 BEEP
1110 DISP " DO YOU WANT A MODE LEGEND? (Y OR N) "
1120 INPUT Z$
1130 IF Z$<>"Y" THEN 1210
1140 DISP " INPUT MODE"
1150 INPUT H$
1160 LOCATE 35,115,30,95
1170 SCALE 0,F,LOG(H/1000),LOG(H*2)
1180 MOVE .5*F,LOG(1.3*H)
1190 LORG 5
1200 LABEL "MODE - ",H$
1210 LINETYPE 1
1220 LOCATE 16,122,20,95
1230 FRAME
1240 FRAME
1250 LOCATE 15,123,19,96
1260 FRAME
1270 FRAME
1280 CLEAR
1290 DISP " END"
1300 END
```

F. PHASE (PHASE plotter)

```
10 DISP " INPUT NAME OF PHASE DATA STORAGE FILE"
20 INPUT R$
30 DIM B(140),C$[50]
40 ASSIGN# 1 TO R$
50 FOR I=1 TO 128
60 READ# 1 ; B(I)
70 NEXT I
80 READ# 1 ; F
90 K=1280
100 ASSIGN# 1 TO *
110 S=200
120 PLOTTER IS 705
130 LOCATE 35,115,30,90
140 CLEAR
150 CLEAR
160 BEEP
170 DISP " DO YOU WANT A GRAPH PLOTTED? (Y OR N)"
180 INPUT V$
190 IF V$="N" THEN 790
200 DISP " INPUT LINETYPE BY NUMBER"
210 INPUT D
220 W=1
230 X=50
240 SCALE 0,F,(S-X*8)*W,S*W
250 FXD 0,0
260 CLEAR
270 BEEP
280 DISP " DO YOU NEED AXES AND AXIS LABELS? (Y OR N)"
290 INPUT R$
300 IF R$="N" THEN 350
310 LAXES -F/10,X*W,0,(S-X*8)*W
320 XAXIS 0,F/10
330 XAXIS 200,F/10
340 YAXIS F,50
350 MOVE 0,B(1)
360 LINETYPE D,1
370 FOR I=2 TO K/10
380 PLOT (I-1)*F/(K/10),B(I),-1
390 NEXT I
400 IF R$="N" THEN 480
410 MOVE 3*F/10,(S-X*8-X)*W
420 LORG 1 @ CSIZE 3,1,0
430 LABEL "FREQUENCY (HZ)"
440 MOVE -F/8,(S-X*8+2*X)*W
450 DEG @ LDIR 90
```

```
460 LABEL "PHASE (DEG)"
470 MOVE 0,(S-X*10)*W
480 LDIR 0
490 CLEAR
500 BEEP
510 DISP " WOULD YOU LIKE A LEGEND FOR THE PLOT? (Y OR N)?"
520 INPUT T$
530 IF T$="N" THEN 690
540 DISP " POSITION 1 OR 2? "
550 INPUT Y
560 DISP " INPUT LEGEND LABLE"
570 INPUT Z$
580 LORG 1 @ CSIZE 2.1,0
590 IF Y=2 THEN 650
600 MOVE F/2,165
610 DRAW .62*F,165
620 MOVE .63*F,165
630 LABEL Z$
640 GOTO 690
650 MOVE F/2,140
660 DRAW .62*F,140
670 MOVE .63*F,140
680 LABEL Z$
690 LOCATE 18,122,20,95
700 LINETYPE 1
710 IF R$="N" THEN 780
720 FRAME
730 FRAME
740 LOCATE 17,123,19,96
750 FRAME
760 FRAME
770 CLEAR
780 BEEP
790 DISP "DO YOU WANT PRINTED OUTPUT Y OR N ?"
800 INPUT Q$
810 IF Q$="N" THEN 890
820 IMAGE "  FREQ        PHASE"
830 PRINT USING 820
840 FOR J=1 TO 128
850 F2=(J-1)*F/127
860 PRINT USING 870 ; F2,B(J)
870 IMAGE ZZZ.DD,6X,SZZZ.DD
880 NEXT J
890 END
```

G. GRAD (thermal neutron flux GRADient calculator)

```
10 DIM M(10),M1(10),T2(10),T3(10),A(10),A1(10),P(10),P1(10),
P2(10),P3(10),U(10),C(10),C1(10)
20 N=9
30 X1=6.559E21
40 V=0
50 E=0
60 L1=.00001515
70 CLEAR
80 BEEP
90 DISP " INPUT IRRADIATION TIME IN SECONDS"
100 INPUT T
110 BEEP
120 DISP "INPUT COUNTING TIME IN SECONDS"
130 INPUT T1
140 Q1=1-EXP(-1*L1*T)
150 BEEP
160 DISP " INPUT BARE BACKGROUND AND CADMIUM BACKGROUND"
170 INPUT B,B1
180 CLEAR
190 BEEP
200 DISP " STARTING WITH THE NORTH OR EAST MOST PIECE, INPUT
 THE MASS IN GRAMS, WAIT TIME IN"
210 DISP "SECONDS, AND COUNT FOR EACH WIRE PIECE GOING FROM
NORTH TO SOUTH OR EAST TO WEST."
220 FOR I=1 TO N
230 INPUT M(I),T2(I),C(I)
240 A(I)=(C(I)-B)/T1
250 Q2=EXP(-1*L1*T2(I))
260 P(I)=A(I)/(M(I)*Q1*Q2)
270 NEXT I
280 CLEAR
290 BEEP
300 DISP " IN THE SAME FORMAT AS ABOVE,INPUT THE DATA FOR TH
E CADMIUM-COVERED PIECES "
310 FOR I=1 TO N
320 INPUT M1(I),T3(I),C1(I)
330 A1(I)=(C1(I)-B1)/T1
340 Q2=EXP(-1*L1*T3(I))
350 P1(I)=A1(I)/(M1(I)*Q1*Q2)
360 P2(I)=P(I)/P1(I)
370 P3(I)=(P2(I)-1)/P2(I)*P(I)
380 E=E+P3(I)
390 NEXT I
400 V=E/N
410 FOR I=1 TO N
420 U(I)=P3(I)/V
```

```
430 NEXT I
440 PRINTER IS 710,132
450 PRINT "                    BARE DATA "
460 IMAGE "POSITION    MASS(G)     WAIT TIME(S)     COUNT "
470 PRINT USING 460
480 FOR I=1 TO N
490 IMAGE 3X,D,7X,D.DDE,5X,D.DDE,4X,D.DDE
500 PRINT USING 490 ; I,M(I),T2(I),C(I)
510 NEXT I
520 PRINT
530 PRINT "                CADMIUM COVERED DATA"
540 PRINT USING 460
550 FOR I=1 TO N
560 PRINT USING 490 ; I,M1(I),T3(I),C1(I)
570 NEXT I
580 PRINT
590 PRINT "POSITION   COR BARE COUNT     COR CD COUNT     CD
 RAT    REL THER FLUX"
600 FOR I=1 TO N
610 IMAGE 3X,D,9X,D.DDE,9X,D.DDE,8X,D.DDE,8X,D.DDDE
620 PRINT USING 610 ; I,P(I),P1(I),P2(I),U(I)
630 NEXT I
640 PRINT
650 CLEAR
660 BEEP
670 DISP " WOULD YOU LIKE A PLOT(Y OR N)? "
680 INPUT R$
690 IF R$="N" THEN 1380
700 PLOTTER IS 705
710 LOCATE 35,115,30,90
720 BEEP
730 DISP " INPUT HIGHEST AND LOWEST VALUES FOR VERTICAL AXIS
"
740 INPUT H,L
750 S=H-L
760 BEEP
770 DISP " INPUT MODE "
780 INPUT Y
790 IF Y=1 THEN J$="NORTH"
800 IF Y=1 THEN K$="SOUTH"
810 IF Y=2 THEN J$="EAST"
820 IF Y=2 THEN K$="WEST"
830 SCALE -4.5,4.5,L,H
840 FXD 1,3
850 LAXES -1,S/10,-4.5,L
860 XAXIS H,1
870 YAXIS 4.5,S/10
880 FOR I=1 TO N
890 W=I-5.5
900 IF I=1 THEN 940
910 IF U(I)<U(I-1) THEN 940
```

```
920 MOVE W,U(I-1)
930 DRAW W,U(I)
940 MOVE W,U(I)
950 DRAW W+1,U(I)
960 IF I=N THEN 980
970 DRAW W+1,L
980 NEXT I
990 PENUP
1000 MOVE -1.5,L-S/8
1010 LORG 1 @ CSIZE 3.1,0
1020 LABEL "DISTANCE (CM)"
1030 MOVE -6,L+S/2 @ LORG 4
1040 DEG @ LDIR 90
1050 LABEL "RELATIVE THERMAL FLUX"
1060 LDIR 0
1070 LOCATE 35,115,30,96
1080 SCALE -4.5,4.5,L,L+1.1*S
1090 MOVE -4.5,1.05*S+L
1100 DRAW -3.5,1.05*S+L
1110 MOVE -4.5,1.05*S+L
1120 DRAW -4.25,1.03*S+L
1130 MOVE -4.5,1.05*S+L
1140 DRAW -4.25,1.07*S+L
1150 MOVE -3.38,1.05*S+L @ LORG 2
1160 CSIZE 2,1,0
1170 LABEL J$
1180 MOVE 3.5,1.05*S+L
1190 DRAW 4.5,1.05*S+L
1200 DRAW 4.25,1.03*S+L
1210 MOVE 4.5,1.05*S+L
1220 DRAW 4.25,1.07*S+L
1230 MOVE 3.38,1.05*S+L @ LORG 8
1240 LABEL K$
1250 MOVE 3.38,1.05*S+L @ LORG 8
1260 CLEAR
1270 BEEP
1280 DISP " INPUT MODE LEGEND"
1290 INPUT O$
1300 MOVE 0,1.05*S+L @ LORG 5
1310 LABEL "MODE - ",O$
1320 LOCATE 16,122,20,95
1330 FRAME
1340 FRAME
1350 LOCATE 15,123,19,96
1360 FRAME
1370 FRAME
1380 CLEAR
1390 BEEP
1400 DISP " AGAIN ? (Y OR N) "
1410 INPUT Z$
1420 IF Z$="Y" THEN 70
```

H. ACT (neutron ACTivation calculator)

```
0001 H1=6.481E+24
0002 L1=1.461E+24
0003 H3=1.913E+24
0004 H4=8.254E+24
0005 L3=1.1377E+24  :  REM NC3L
0006 L5=5.0037E+23  :  REM NC5L
0007 L4=0.0         :  REM NZ4L
0008 H4=6.714E+24
0009 L8=0.0         :  REM NZ8L
0010 H8=2.444E+23
0011 C3=4.5E-24     :  REM SGAC3
0012 C5=2.300E-24   :  REM SGAC5
0013 Z4=8.200E-25   :  REM SGAZ4
0014 G8=1.000E-24   :  REM SGAZ8G
0015 I8=9.000E-26   :  REM SGAZ8I
0016 A =134.4       :  REM THFA
0017 C4=45756.0
0018 C6=306.0       :  REM THFC6
0019 Z5=2.1064E+7   :  REM THFZ5
0020 G9=3420.0
0021 I9=49680.0     :  REM THFZ9I
0022 F1=0.0
0023 F2=0.0
0024 S1=0.0
0025 A2=0.0
0026 A3=0.0
0027 A4=0.0
0028 A5=0.0
0029 A6=0.0
0030 A7=0.0
0031 G =.233E-24    :  REM SGAA
0100 REM USER INPUT
0101 INPUT "INPUT MAXIMUM ALLOWABLE ACTIVATION IN CURIES",A1
0105 PRINT   "
0110 INPUT "INPUT DEPARTURE TIME (MINUTES FROM START OF RUN)".T1
0115 PRINT " "
0120 INPUT "INPUT POWER RATIO",R1
0125 PRINT " "
0130 PRINT "INPUT REACTOR PERIOD IN SECONDS."
0135 INPUT "USE 0 IF NO CHANGE IS DESIRED.",T
0140 PRINT " "
0145 INPUT "INPUT INITIAL REACTOR POWER IN WATTS",P0
0150 PRINT " "
0200 REM CALCULATION OF FLUXES
0205 P1=P0*R1
```

```
0210 F3=F1
0215 F4=F2
0220 F1=1.0E+7*P1
0225 F2=5.0E+6*P1
0250 REM CALCULATION OF STEP TIME AND ARRIVAL TIME
0255 S2=S1
0260 IF R1=1.00 THEN 270
0265 S1=(T1*60.0)+((T+(R1*(T*LOG(R1)-T)))/(R1-1.0))
0270 T2=(T1*60.0)+(T*LOG(R1))
0275 IF R1<>1.00 THEN 305
0280 S1=T1*60.0
0300 REM CALCULATION OF TIME CONSTANTS
0305 M1=LOG(2.0)/A
0310 M2=LOG(2.0)/C4
0315 M3=LOG(2.0)/C6
0320 M4=LOG(2.0)/Z5
0325 M5=LOG(2.0)/G9
0330 M6=LOG(2.0)/I9
0350 REM CALCULATION OF ACTIVATIONS UP TO POWER CHANGE
0355 B2=A2
0360 B3=A3
0365 B4=A4
0370 B5=A5
0375 B6=A6
0380 B7=A7
0385 A2=(H1*G*F1)+(L1*G*F2)
0390 A3=B3+(L3*C3*F4*M2*(S1-S2)) + (H3*C3*F3*M2*(S1-S2))
0395 A4=(L5*C5*F2) + (H5*C5*F1)
0410 A5=B5 + (L4*Z4*F4*M4*(S1-S2)) + (H4*Z4*F3*M4*(S1-S2))
0420 A7=B7 + (L8*I8*F4*M6*(S1-S2)) + (H8*I8*F3*M6*(S1-S2))
0430 A6=L8*G8*F4*(1.-EXP((-1.0)*M5*(S1-S2))) + B6
0435 A6=A6 + (H8*G8*F3*(1.-EXP((-1.0)*M5*(S1-S2))))
0450 REM PRINTOUT OF DATA
0455 T2=T2/60.0
0460 S3=S1/60.0
0465 D2=A2/3.7E+10
0470 D3=A3/3.7E+10
0475 D4=A4/3.7E+10
0480 D5=A5/3.7E+10
0485 D6=A6/3.7E+10
0490 D7=A7/3.7E+10
0495 D8=D2+D3+D4+D5+D6+D7
0500 PRINT " "
0505 PRINT "DEPARTURE TIME IN MINUTES =",T1
0510 PRINT " "
0515 PRINT "ARRIVAL TIME IN MINUTES =",T2
0520 PRINT " "
0525 PRINT "INITIAL POWER IN WATTS=",P0
0530 PRINT " "
0535 PRINT "FINAL POWER IN WATTS=",P1
0540 PRINT " "
```

```
0545 PRINT "POWER RATIO =",R1
0550 PRINT " "
0555 PRINT "REACTOR PERIOD IN SECONDS=",T
0560 PRINT " "  :  PRINT " "
0565 PRINT "            ACTIVITIES BY ISOTOPE"
0570 PRINT "            ********** ** *******"
0575 PRINT " "
0580 PRINT " ACTIVITIES ARE FOR A TIME IN MINUTES OF", S3
0585 PRINT " "
0590 PRINT " ISOTOPE              ACTIVITY IN CURIES"
0595 PRINT " *******              ******** ** ******"
0600 PRINT " "
0605 PRINT "  AL-28                 ",D2
0610 PRINT " "
0615 PRINT "  CU-64                 ",D3
0620 PRINT " "
0625 PRINT "  CU-66                 ",D4
0630 PRINT " "
0635 PRINT "  ZN-65                 ",D5
0640 PRINT " "
0645 PRINT "  ZN-69G                ",D6
0650 PRINT " "
0655 PRINT "  ZN-69I                ",D7
0660 PRINT " "
0665 PRINT "  TOTAL                 ",D8
0670 IF D8>A1 THEN 765
0675 IF P1<1.0 THEN 920
0700 REM CALCULATION OF MAXIMUM TIME AT PRESENT POWER
0705 N=(A1-(D2+D3+D4+D5+D6+D7))*3.7E+10
0710 N1=C3*M2*((L3*F2)+(H3*F1))
0715 N2=Z4*M4*((L4*F2)+(H4*F1))
0720 N3=G8*M5*((L8*F2)+(H8*F1))
0725 N4=I8*M6*((L8*F2)+(H8*F1))
0730 N5=N1+N2+N3+N4
0735 T3=(S1+(N/N5))/60.0
0740 PRINT " "
0745 PRINT "TIME IN MINUTES AT WHICH THE MAXIMUM ACTIVATION LEVEL WILL"
0750 PRINT "BE REACHED AT THE NEW POWER IS",T3
0760 GOTO 830
0765 PRINT "THIS POWER CHANGE WILL IMMEDIATELY CAUSE THE ACTIVITIES TO"
0770 PRINT "EXCEED THE GIVEN MAXIMUM.  PLEASE INPUT NEW DATA."
0780 A2=B2
0785 A3=B3
0790 A4=B4
0795 A5=B5
0800 A6=B6
0805 A7=B7
0810 F2=F4
0815 F1=F3
0820 S1=S2
0825 GOTO 105
```

```
0830 PRINT " "
0835 PRINT "IF THIS DATA IS ACCEPTABLE AND THE POWER CHANG IS MADE, TYPE"
0840 INPUT "'1'. IF NEW DATA IS TO BE TESTED, TYPE '2'.",M
0845 IF M=1 THEN 105
0850 IF M=2 THEN 870
0855 PRINT " "
0860 PRINT " INCORRECT RESPONSE - TYPE 1 OR 2"
0865 GOTO 830
0870 A2=B2
0875 A3=B3
0880 A4=B4
0885 A5=B5
0890 A6=B6
0895 A7=B7
0900 F2=F4
0905 F1=F3
0910 S1=S2
0915 GOTO 105
0920 PRINT " "
0925 PRINT "POWER IS LESS THAN 1 WATT. IS THE RUN FINISHED (TYPE 0) OR WILL
0930 INPUT "IT BE CONTINUED (TYPE 1)",K
0935 IF K=1 THEN 705
0940 IF K=0 THEN 999
0945 PRINT "INCORRECT RESPONSE - TYPE 0 OR 1"
0950 GOTO 920
0999 END
```